Computer Methods in Applied Mechanics and Engineering 450 (2026) 118522

Contents lists available at ScienceDirect

Comput. Methods Appl. Mech. Engrg.

journal homepage: www.elsevier.com/locate/cma

Scalable augmented Lagrangian preconditioners for fictitious domain problems ⋆

Michele Benzi [a], Marco Feder [b], Luca Heltai [b], Federica Mugnaioni [a,*]

[a] Scuola Normale Superiore, Piazza dei Cavalieri, 7, 56126 Pisa, Italy
[b] Department of Mathematics, University of Pisa, Largo B. Pontecorvo, 5, Pisa 56127, Italy

ARTICLE INFO

Keywords:
Preconditioning
Iterative solvers
Fictitious domain method
Non-matching meshes
Finite element method

ABSTRACT

We present preconditioning techniques to solve linear systems of equations with a block two-by-two and three-by-three structure arising from finite element discretizations of the fictitious domain method with Lagrange multipliers. In particular, we propose two augmented Lagrangian-based preconditioners to accelerate the convergence of iterative solvers for such classes of linear systems. We consider two relevant examples to illustrate the performance of these preconditioners when used in conjunction with flexible GMRES: the Poisson and the Stokes fictitious domain problems. A spectral analysis is established for both exact and inexact versions of the preconditioners. We show the effectiveness of the proposed approach and the robustness of our preconditioning strategy through extensive numerical tests in both two and three dimensions.

1. Introduction

Over the years, several numerical approaches have been developed to address problems involving overlapping or non-matching computational meshes. Among these, we highlight a small selection of well-established methods: the Immersed Boundary Method [1] (IBM), the Finite Cell Method [2] (FCM), the Cut Finite Element Method [3] (CutFEM), and the Fictitious Domain approach [4–6] (FD). These methods differ in how they treat cells and degrees of freedom near the interface. CutFEM and FCM involve adjustments to the degrees of freedom and integral routines, since the degrees of freedom on cut cells are duplicated across the interface, and bulk integrals are recomputed over the polygonal or polytopal shapes resulting from the intersections of the elements with the cutting interface. For moving interface problems, such as in fluid-structure interactions, this may require recomputing the bulk contribution at each time step. In contrast, FD methods treat all cells in the same way without duplicating degrees of freedom, although this comes at the price of lower global order of convergence, which has been shown to be only a local effect near the interface [7]. Furthermore, when using Lagrange multipliers in fictitious domain methods, coupling operators are assembled to encode interactions between basis functions defined on non-matching and overlapping meshes [8]. Nevertheless, integration issues are limited to the coupling term only, making these methods attractive for moving interface problems by avoiding recomputation of bulk integrals. Recent developments have shown that it is also possible to compute these integrals without explicitly dealing with mesh intersections, and this does not deteriorate the convergence properties of the method [9]. Moreover, it is robust with respect to small cuts [10], while CutFEM and FCM may require additional stabilization in such cases. Therefore, when the coupling between the bulk and the interface problems

⋆ Dedicated to the memory of Howard Elman

* Corresponding author.
E-mail addresses: michele.benzi@sns.it (M. Benzi), marco.feder@dm.unipi.it (M. Feder), luca.heltai@unipi.it (L. Heltai), federica.mugnaioni@sns.it (F. Mugnaioni).

https://doi.org/10.1016/j.cma.2025.118522
Received 15 April 2025; Received in revised form 3 October 2025; Accepted 23 October 2025

can be modeled through a Lagrange multiplier, the fictitious domain method offers a viable alternative which is generally simpler to implement, and may be computationally more efficient, especially in the presence of moving domains. Several aspects of these methods have been addressed in the literature. For example, stabilization of the method when used in conjunction with CutFEM has been presented in [11], the impact of different types of coupling operators on the convergence of the resulting method has been analyzed in [9,12], while possible strategies for the implementation of these operators in parallel computing environments, where the non-overlapping meshes are generally distributed with different partitioning, have been presented in [13,14].

The major drawback of using the Lagrange multiplier based Fictitious Domain method remains the computational demands of solving the resulting large-scale problems, both in terms of time and memory. In this work, we answer this challenge by proposing efficient preconditioning techniques that significantly reduce computational costs while maintaining robustness and scalability.
We focus on two model problems stemming from the application of the fictitious domain approach to the Poisson and Stokes problem. After discretization, the resulting linear systems exhibit the following two-by-two and three-by-three block structures:

$$\begin{bmatrix} A & C^T \\ C & 0 \end{bmatrix} \begin{bmatrix} u \\ \lambda \end{bmatrix} = \begin{bmatrix} f \\ g \end{bmatrix} \quad \text{and} \quad \begin{bmatrix} A & B^T & C^T \\ B & 0 & 0 \\ C & 0 & 0 \end{bmatrix} \begin{bmatrix} u \\ p \\ \lambda \end{bmatrix} = \begin{bmatrix} f \\ 0 \\ g \end{bmatrix}, \tag{1}$$

where $A \in \mathbb{R}^{n\times n}$ is symmetric positive definite (SPD), $B \in \mathbb{R}^{m\times n}$ and $C \in \mathbb{R}^{l\times n}$.
Two-by-two block linear systems of this type are an example of saddle point problems which arise in many areas of computational science and engineering. In [15], a wide variety of technical and scientific applications leading to these saddle point problems is reviewed, including mixed finite element methods and linear and nonlinear optimization. Similarly, three-by-three block linear systems of this form arise, for instance, in finite element modelling of potential fluid flow problems [16] or elasticity problems [17]. The large-scale saddle point problems in (1) make the use of direct solvers prohibitive, as they do not scale well with the size of the problem, in terms of both computational cost and memory usage. This is particularly evident when solving problems that result from discretizing partial differential equations in three-dimensional space. Moreover, as the mesh size approaches zero, the condition number of the system matrices increases, leading to a deterioration in the convergence rate of iterative methods. Designing a suitable preconditioner is crucial to reduce or even eliminate this dependency on the mesh size. Developing robust solvers is also essential for efficiently handling computations with a large number of time steps and fine spatial discretizations within a reasonable timeframe.
Regarding the two-by-two block linear system of saddle point type in (1), a large selection of solution methods is reviewed in [15], which also provides a detailed survey on preconditioners. In computational fluid dynamics, block diagonal and block triangular preconditioners are particularly popular [18]. The effectiveness of such preconditioners depends on the availability of good approximations for both the (1,1)-block A and the Schur complement $S = CA^{-1}C^T$. However, finding a suitable approximation for the dense matrix S is especially challenging in the context of interface non-fitted meshes; difficulties arise because the matrix C in (1) does not consist of integrals defined on the *same* computational mesh, but rather on two arbitrarily overlapping grids. Preconditioning strategies for unfitted methods are an active area of research, and have been explored in [19–21], to mention a few. However, to the best of our knowledge, for the fictitious domain with Lagrange multipliers method, it remains unclear how to construct a good approximation for the algebraic Schur complement and to which matrix it is spectrally equivalent. For this reason, in this paper, we propose an effective augmented Lagrangian-based preconditioner that eliminates the need for a good approximation to the dense Schur complement matrix. On the other hand, as shown in [22,23], in the framework of fitted (or matching) meshes, the algebraic Schur complement S is tightly related to the continuous properties of the trace operator, requiring the computation of the action of fractional operators. A technique to overcome the computational burden associated with this matter is presented in [24].
Recently, several studies have focused on iterative methods and robust preconditioners for solving three-by-three block systems [25–28]. In [25], various block diagonal and block triangular preconditioners for Krylov subspace methods are described and analyzed for double saddle point systems with the same structure as the one in (1). Several alternatives have been proposed in the literature, particularly for cases where the (3,3)-block is non-zero [29–33]. In addition, preconditioners for Fictitious Domain with Distributed Lagrange Multipliers (FD-DLM) formulations have been recently explored in [34–36], while Uzawa iterative methods were presented in [37,38]. Most of the available preconditioners, such as those proposed in [25], require finding an approximation for both Schur complements $S_B = BA^{-1}B^T$ and $S_C = CA^{-1}C^T$. We note that in our formulation the matrices A and B in (1) are the same as those in the problem without an immersed boundary. Therefore, existing literature on how to approximate S_B can be directly used (for instance, in the Stokes scenario, A and B correspond exactly to the discrete Laplacian and the discrete divergence of the classical Stokes problem). The main challenge is therefore related to finding approximations for S_C. To address this issue, we propose an extension of the augmented Lagrangian (AL)-based preconditioner proposed for the two-by-two block linear system, as an effective preconditioner for the three-by-three block case.

In both cases, we follow the main ideas of augmented Lagrangian preconditioners in the context of stable finite element discretizations of the Oseen and Navier-Stokes equations [39,40], and derive an equivalent AL formulation for the problems at hand. The global linear system of equations is solved using a (flexible) Krylov subspace method. In this work, we use Flexible GMRES (FGMRES) [41] since the preconditioner is a variable one due to the way the (1,1)-block is approximately inverted. As previously indicated, to illustrate the performance of the proposed preconditioners in the context of fictitious domain methodologies, we consider two relevant test problems: the Poisson fictitious domain problem, which results in the two-by-two block linear system in (1), and the Stokes fictitious domain problem, where the imposition of a constraint on the velocity field on the immersed boundary yields a *double* saddle point problem as the one in (1). For the first model problem, the two-by-two block linear system is non-singular, whereas the system matrix in the second case may be singular (due to the rank deficiency of B) if Dirichlet boundary conditions are applied on the whole boundary, leaving the scalar pressure field defined up to a constant.

In contrast to classical preconditioners for Stokes problems, where only the mass matrix on the pressure space is exploited while building the augmented block [39], also the mass matrix on the space of the Lagrange multiplier is needed when considering a fictitious domain formulation. We provide a spectral analysis of the proposed AL preconditioner for the Stokes problem, assuming both exact and inexact solves (using similar arguments as in [28]). Analogous considerations hold for the Poisson case. Through extensive numerical experiments, uniform convergence with respect to the discretization parameters is observed. Moreover, having in mind three-dimensional scenarios where the computational complexity of sparse direct solvers for inverting individual blocks of the preconditioner soon becomes prohibitive, we have investigated the performance of our solvers when only inner iterative solvers are employed, confirming the good convergence properties. We provide a distributed memory implementation of the proposed methodology using the DEAL.II finite element library [42,43].

The work is structured as follows. In Section 2, we introduce the relevant notation and setup through a Poisson problem with an internal boundary, and derive an augmented Lagrangian-based preconditioner for the model problem. In Section 3, we extend the same technique to the Stokes system and perform a spectral analysis of the proposed preconditioner in Section 4. In Section 5, we discuss in detail the eigenvalue distribution of the preconditioned matrix when an inexact version of the proposed AL-based preconditioner is used, while Section 6 provides several numerical experiments to validate the robustness of our methodology across different scenarios. Finally, Section 7 summarizes our conclusions and points to further research directions.

2. Poisson fictitious domain problem and notation

Let ω be a closed and bounded domain of $\mathbb{R}^d$, $d = 2, 3$, with Lipschitz continuous boundary $\Gamma := \partial\omega$, and $\Omega \subset \mathbb{R}^d$ a Lipschitz domain such that $\omega \Subset \Omega$. We consider the Poisson model problem

$$\begin{cases} -\Delta u = f & \text{in} \quad \Omega \setminus \Gamma, \\ u = g & \text{on} \quad \Gamma, \\ u = 0 & \text{on} \quad \partial\Omega, \end{cases} \tag{2}$$

for given data $f \in L^2(\Omega)$ and $g \in H^{\frac{1}{2}}(\Gamma)$. Throughout this work we refer to Ω as the *background* domain, while we refer to ω as the *immersed* domain, and Γ as the *immersed boundary*. Hence, Γ is a subset of Ω of codimension one (a surface in dimension three or a curve in dimension two). The rationale behind this setting is that it allows solving problems in a complex and possibly time-dependent domain ω, by embedding it in a simpler background domain Ω – typically a box – and imposing some constraints on the immersed boundary Γ. For the sake of simplicity, we consider the case in which the immersed domain is *entirely* contained in the background domain, but more general configurations may be considered. A prototypical configuration is shown in Fig. 1.

Given a domain $D \subset \mathbb{R}^d$ and a real number $s \geq 0$, we denote by $\|\cdot\|_{s,D}$ the standard Sobolev norm of $H^s(D)$. In particular, $\|\cdot\|_{0,D}$ stands for the L^2-norm stemming from the standard L^2-inner product $(\cdot,\cdot)_D$ on D. Finally, with $\langle\cdot,\cdot\rangle_\Gamma$ we denote the standard duality pairing between $H^{\frac{1}{2}}(\Gamma)$ and its dual. At the discrete level, it can be evaluated using the scalar product in $L^2(\Gamma)$, provided that $\Lambda_h \subset L^2(\Gamma)$. As ambient spaces, we consider

$$V(\Omega) := H_0^1(\Omega) = \{v \in H^1(\Omega) : v_{|\partial\Omega} = 0\},$$

and

$$\Lambda(\Gamma) := H^{-\frac{1}{2}}(\Gamma),$$

which guarantee the well-posedness of the continuous problem thanks to the fulfillment of the *ellipticity on the kernel* and the *inf-sup* condition [44].

Problem (2) can be written as a constrained minimization problem by introducing the Lagrangian $\mathcal{L} : V(\Omega) \times \Lambda(\Gamma) \to \mathbb{R}$ defined as

$$\mathcal{L}(v, \mu) := \frac{1}{2}(\nabla v, \nabla v)_\Omega - (f, v)_\Omega + \langle \mu, v - g\rangle_\Gamma. \tag{3}$$

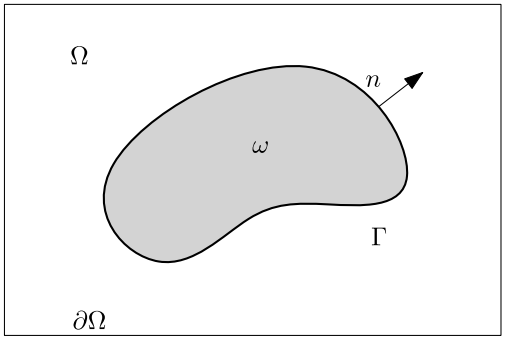

Fig. 1. Model problem setting, with immersed domain ω, immersed boundary Γ, and background domain Ω.

Looking for stationary points of $\mathcal{L}$ gives the following saddle point problem of finding a pair $(u, \lambda) \in V(\Omega) \times \Lambda(\Gamma)$ such that

$$(\nabla u, \nabla v)_\Omega + \langle \lambda, v \rangle_\Gamma = (f, v)_\Omega \qquad \forall v \in V(\Omega), \tag{4}$$

$$\langle \mu, u \rangle_\Gamma = \langle \mu, g \rangle_\Gamma \qquad \forall \mu \in \Lambda(\Gamma), \tag{5}$$

which in operator form reads as

$$\begin{bmatrix} A & C^T \\ C & 0 \end{bmatrix} \begin{bmatrix} u \\ \lambda \end{bmatrix} = \begin{bmatrix} F \\ G \end{bmatrix},$$

where

$$A : V(\Omega) \to V(\Omega)' \quad \langle Au, v \rangle_{V(\Omega)', V(\Omega)} = (\nabla u, \nabla v)_\Omega,$$

$$C : V(\Omega) \to \Lambda(\Gamma)' \quad \langle Cv, \lambda \rangle_{\Lambda(\Gamma)', V(\Omega)} = \langle \lambda, v \rangle_\Gamma,$$

$$F : V(\Omega) \to \mathbb{R} \quad F(v) = (f, v)_\Omega,$$

$$G : \Lambda(\Gamma) \to \mathbb{R} \quad G(\mu) = \langle \mu, g \rangle_\Gamma.$$

As is clear from the previous paragraph, we use normal font to denote linear operators, e.g. A, while matrices and vectors are denoted by the sans serif font, e.g., A and x, respectively. Moreover, we will use a calligraphic font to denote block matrices associated with the saddle point system, e.g., $\mathcal{A}$. We will use the letter λ to denote both the Lagrange multiplier and a generic eigenvalue of a matrix. The different meaning will be clear from the context and no confusion should arise.

2.1. Finite element discretization and mesh assumptions

We discretize the computational meshes associated with the background domain Ω and with the immersed boundary Γ in an *unfitted* or *non-matching* way, in the sense that the two computational grids are constructed independently, and no alignment conditions are asked. The computational meshes Ω_h and Γ_h consist of a finite number N_Ω and N_Γ of disjoint elements T_i and K_i such that $\{T_i\}_{1 \le i \le N_\Omega}$ and $\{K_i\}_{1 \le i \le N_\Gamma}$ form a partition of Ω and Γ, i.e. $\overline{\Omega} = \bigcup_{i=1}^{N_\Omega} T_i$, and $\overline{\Gamma} = \bigcup_{i=1}^{N_\Gamma} K_i$. When $d = 2$, Ω_h will be a quadrilateral mesh and Γ_h a mesh composed by straight line segments. For $d = 3$, Ω_h will be a hexahedral mesh and Γ_h is a surface mesh whose elements are quadrilaterals embedded in the three-dimensional space. We denote by h_Ω and h_Γ the mesh sizes of Ω_h and Γ_h, respectively. For simplicity, we assume that the mesh sizes h_Ω and h_Γ are small enough so that the geometrical error is negligible with respect to the discretization error. Furthermore, we assume Γ_h to be a quasi-uniform discretization of Γ. In practice, we will consider meshes Γ_h with a uniform mesh-size, using background meshes Ω_h that may be locally refined in the vicinity of Γ_h to capture the geometry of the immersed boundary.

We consider the finite element discretization of $V(\Omega)$ based on linear standard Lagrange finite elements, namely

$$V_h := \{v_h \in H_0^1(\Omega) : \, v_h|_T \in \mathcal{Q}^1(T), \forall T \in \Omega_h\}, \tag{6}$$

where $\mathcal{Q}^1(T)$ denotes the space of polynomials of degree 1 in each variable on the element T. For the Lagrange multiplier space $\Lambda(\Gamma)$ we set

$$\Lambda_h := \{\mu_h \in L^2(\Gamma) : \, \mu_h|_K \in \mathcal{Q}^1(K), \forall K \in \Gamma_h\}. \tag{7}$$

Given basis functions $\{\varphi_i\}_{i=1}^n$ and $\{\psi_\alpha\}_{\alpha=1}^l$ such that $V_h := \mathrm{span}\{\varphi_i\}_{i=1}^n$ and $\Lambda_h := \mathrm{span}\{\psi_\alpha\}_{\alpha=1}^l$, we have that the discrete version of (4), (5) can be written as the following algebraic problem with unknowns u and λ:

$$\begin{bmatrix} \mathsf{A} & \mathsf{C}^\mathsf{T} \\ \mathsf{C} & 0 \end{bmatrix} \begin{bmatrix} \mathsf{u} \\ \lambda \end{bmatrix} = \begin{bmatrix} \mathsf{f} \\ \mathsf{g} \end{bmatrix} \quad \text{or} \quad \mathcal{A}\mathsf{x} = \mathsf{b}, \tag{8}$$

where

$$\begin{aligned} \mathsf{A}_{ij} &= (\nabla \varphi_j, \nabla \varphi_i)_\Omega && i, j = 1, \dots, n \\ \mathsf{C}_{\alpha i} &= \langle \varphi_i, \psi_\alpha \rangle_\Gamma && i = 1, \dots, n \quad \alpha = 1, \dots, l \\ \mathsf{f}_i &= (f, \varphi_i)_\Omega && i = 1, \dots, n \\ \mathsf{g}_\alpha &= \langle \psi_\alpha, g \rangle_\Gamma && \alpha = 1, \dots, l. \end{aligned}$$

Note that $\mathsf{A} \in \mathbb{R}^{n \times n}$ is symmetric positive definite and $\mathsf{C} \in \mathbb{R}^{l \times n}$. Next, we recall the following theorem that states the existence, uniqueness, and stability of the discrete solution together with optimal error estimates. The interested reader is referred to [5, Sect. 5], for the details. Notice that C must have full row rank in order to ensure the solvability of the algebraic problem (8), which is guaranteed by the inf-sup condition (9) below.

Proposition 1. *Let V_h and Λ_h be defined as above. If h_Ω / h_Γ is sufficiently small and the mesh Γ_h is quasi-uniform, then there exists β_2 independent of the mesh sizes h_Ω and h_Γ such that the following discrete inf-sup condition holds:*

$$\inf_{\mu_h \in \Lambda_h} \sup_{v_h \in V_h} \frac{\langle \mu_h, v_h \rangle_\Gamma}{||\mu_h||_{-\frac{1}{2}, \Gamma} ||v_h||_{1, \Omega}} \ge \beta_2. \tag{9}$$

Standard theory of saddle point problems [17] yields the following a priori estimate.

Theorem 1. *Let V_h and Λ_h be defined as above. If h_Ω/h_Γ is sufficiently small and the mesh Γ_h is quasi-uniform, then the unique solution $(u_h, \lambda_h) \in V_h \times \Lambda_h$ of the discretization of (4), (5), satisfies*

$$\|u - u_h\|_{1,\Omega} + \|\lambda - \lambda_h\|_{-1/2,\Gamma} \le C \inf_{\substack{v_h \in V_h \\ \mu_h \in \Lambda_h}} \left(\|u - v_h\|_{1,\Omega} + \|\lambda - \mu_h\|_{-1/2,\Gamma} \right), \tag{10}$$

with $C > 0$ a constant independent of the mesh sizes h_Ω and h_Γ.

Remark 1. These results show that the accuracy of the FD method depends on the approximation properties of both the solution and the Lagrange multiplier spaces, provided the continuous and discrete inf-sup conditions hold. In particular, Theorem 1 suggests that discretization spaces should be chosen so that their approximation properties are balanced both in terms of polynomial degrees, and in terms of the mesh ratio; otherwise, the global error is dominated by the least accurate variable, and the inf-sup condition may deteriorate. Indeed, the constant C in (10) is independent of the mesh sizes, but not of their ratio, as the discrete inf-sup condition of the coupling operator reflects this dependence. Hence, no advantage would be gained by choosing a very small or a very large ratio. The proposed preconditioner is designed to be effective under these conditions, ensuring robust convergence and a consistently low iteration count.

2.2. Augmented Lagrangian preconditioner

We present our augmented Lagrangian-based preconditioner for the model problem (2) discretized by stable finite element pairs. Our derivation closely follows early works on augmented Lagrangian preconditioning for the Oseen problem [39,40].

The idea behind the classical AL approach is to replace the original system (8) with the equivalent formulation

$$\begin{bmatrix} \mathsf{A} + \gamma \mathsf{C}^\mathsf{T}\mathsf{W}^{-1}\mathsf{C} & \mathsf{C}^\mathsf{T} \\ \mathsf{C} & 0 \end{bmatrix} \begin{bmatrix} \mathsf{u} \\ \lambda \end{bmatrix} = \begin{bmatrix} \mathsf{f} + \gamma \mathsf{C}^\mathsf{T}\mathsf{W}^{-1}\mathsf{g} \\ \mathsf{g} \end{bmatrix} \quad \text{or} \quad \mathcal{A}_\gamma \mathsf{x} = \hat{\mathsf{b}}, \tag{11}$$

where W is a properly chosen SPD matrix and γ is a positive real number. Having defined the augmented term as $\mathsf{A}_\gamma := \mathsf{A} + \gamma \mathsf{C}^\mathsf{T}\mathsf{W}^{-1}\mathsf{C}$, an ideal preconditioner for problem (11) is given by the block triangular matrix

$$\mathcal{P}_\gamma := \begin{bmatrix} \mathsf{A}_\gamma & \mathsf{C}^\mathsf{T} \\ 0 & -\frac{1}{\gamma}\mathsf{W} \end{bmatrix}. \tag{12}$$

Since A is SPD and C has full row rank, the conditions of Lemma 4.1 in [39] are satisfied, thus $\gamma\mathsf{W}^{-1}$ provides a good approximation for the inverse of the Schur complement $\mathsf{S}_\gamma = \mathsf{C}\mathsf{A}_\gamma^{-1}\mathsf{C}^\mathsf{T}$ when γ is large. However, as γ increases, A_γ becomes increasingly ill conditioned, making it preferable to keep γ at a moderate value. The choice of the user-defined parameter γ is crucial for the performance of the preconditioner. Indeed, it should be selected based on a trade-off between the number of inner iterations required to approximate the action of A_γ^{-1} and the number of outer iterations needed to solve the entire system in (11). Note that the potential benefit of $\mathcal{A}_\gamma$ being symmetric is lost when a nonsymmetric preconditioner, such as the one in (12), is used. However, if good approximations to A_γ and S_γ are available, using a method such as (F)GMRES with block triangular preconditioning will lead to rapid convergence, making the overhead incurred from the use of a non-symmetric solver negligible [15]. In practice, the action of $\mathcal{P}_\gamma^{-1}$ is given by

$$\mathcal{P}_\gamma^{-1} = \begin{bmatrix} \mathsf{A}_\gamma^{-1} & 0 \\ 0 & \mathsf{I}_l \end{bmatrix} \begin{bmatrix} \mathsf{I}_n & \mathsf{C}^\mathsf{T} \\ 0 & -\mathsf{I}_l \end{bmatrix} \begin{bmatrix} \mathsf{I}_n & 0 \\ 0 & \gamma\mathsf{W}^{-1} \end{bmatrix},$$

where I_n and I_l are identity matrices of size n and l, respectively. The last identity implies that the application of the preconditioner to a vector requires one solve with W, and one solve with the augmented term A_γ. On top of that, we observe that this reformulation avoids the need to find a suitable approximation for the dense matrix $\mathsf{S} = \mathsf{C}\mathsf{A}^{-1}\mathsf{C}^\mathsf{T}$, a task that is particularly challenging in the context of interface non-fitted meshes. As already mentioned, the difficulty stems from the fact that the off-diagonal blocks in (8) involve integrals of basis functions that are not defined on the *same* computational mesh, but rather on two grids that may overlap arbitrarily. The choice of the matrix W is crucial for the practical performance and applicability of the preconditioner. We propose to choose

$$\mathsf{W} := \mathsf{M}_\lambda^2, \tag{13}$$

where M_λ is the mass matrix on the immersed space $\Lambda_h \subset \Lambda(\Gamma)$, i.e.

$$\left(\mathsf{M}_\lambda\right)_{\alpha,\beta} := \int_\Gamma \psi_\alpha \psi_\beta, \qquad \alpha, \beta = 1, \dots, l. \tag{14}$$

The reason for this choice will become clear in Section 4, where we discuss the Stokes case. The main idea is that the solutions of the generalized eigenvalue problem

$$\begin{bmatrix} \mathsf{A}_\gamma & \mathsf{C}^\mathsf{T} \\ \mathsf{C} & 0 \end{bmatrix} \begin{bmatrix} \mathsf{x} \\ \mathsf{y} \end{bmatrix} = \lambda \begin{bmatrix} \mathsf{A}_\gamma & \mathsf{C}^\mathsf{T} \\ 0 & -\frac{1}{\gamma}\mathsf{W} \end{bmatrix} \begin{bmatrix} \mathsf{x} \\ \mathsf{y} \end{bmatrix}, \tag{15}$$

are given by $\lambda = 1$ and the associated eigenvector $(\mathsf{x}, -\gamma\mathsf{W}^{-1}\mathsf{C}\mathsf{x})$, or $\lambda = \frac{\gamma \mathsf{x}^\mathsf{T}\mathsf{C}^\mathsf{T}\mathsf{W}^{-1}\mathsf{C}\mathsf{x}}{\mathsf{x}^\mathsf{T}(\mathsf{A}+\gamma\mathsf{C}^\mathsf{T}\mathsf{W}^{-1}\mathsf{C})\mathsf{x}}$, for $\mathsf{x} \notin \ker(\mathsf{C})$. In Section 4, we will prove that choosing $\mathsf{W} := \mathsf{M}_\lambda^2$ ensures that λ remains bounded away from zero uniformly in h_Ω and h_Γ (see Eq. (66)). This result holds for both

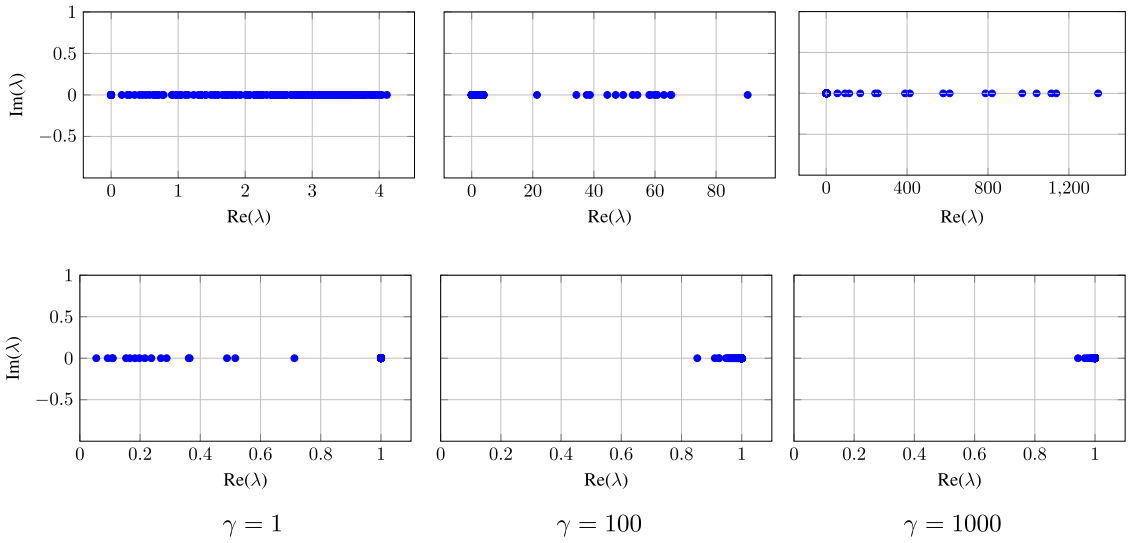

Fig. 2. Spectrum of the *original* matrix $\mathcal{A}_\gamma$ (top row) and $\mathcal{P}_\gamma^{-1}\mathcal{A}_\gamma$ (bottom row) for increasing values of γ.

the Poisson and the Stokes cases.

Due to the expensive solve associated especially with A_γ, the preconditioner $\mathcal{P}_\gamma$ in (12) is only *ideal* and not of practical use. For this reason, it is necessary to replace the exact solves with approximate ones, resulting in a preconditioner which we denote as follows

$$\widehat{\mathcal{P}}_\gamma := \begin{bmatrix} \widehat{\mathsf{A}}_\gamma & \mathsf{C}^\mathsf{T} \\ 0 & -\frac{1}{\gamma}\widehat{\mathsf{W}} \end{bmatrix}, \tag{16}$$

where $\widehat{\mathsf{A}}_\gamma$ and $\widehat{\mathsf{W}}$ are approximations of A_γ and W, respectively, defined through the action of their inverses on vectors. The action of A_γ^{-1} is approximated through the conjugate-gradient (CG) solver preconditioned by a V-cycle of Algebraic MultiGrid (AMG). It is well known that, provided that a flexible GMRES solver is used to solve (11), the inversion of the (1,1)-block of the preconditioner does not need to be done with high accuracy, so the tolerance for this block will be set to a rather loose value in the numerical experiments. Concerning the (2,2)-block, we observe that the number of degrees of freedom (DoF) associated with the immersed space Λ_h is generally much lower than the number of DoF in the background space V_h. Indeed, while on a quasi-uniform mesh the number of background cells in Ω_h scales with $\mathcal{O}(h^{-d})$, the number of facets in Γ_h scales with $\mathcal{O}(h^{-(d-1)})$. This would suggest that sparse direct solvers (such as UMFPACK [45]) could still be employed for the inversion of $\mathsf{W} = \mathsf{M}_\lambda^2$, therefore it is not necessary to find an approximation $\widehat{\mathsf{W}}$ also when the number of DoF in the background is large. When it becomes impractical, we choose to approximate W with a diagonal matrix whose entries are the squares of the main diagonal entries of M_λ, i.e.

$$\widehat{\mathsf{W}} := \mathrm{diag}(\mathsf{M}_\lambda)^2. \tag{17}$$

Notably, if $\widehat{\mathsf{W}}$ is diagonal, the sparsity pattern of the augmented matrix A_γ remains close to the sparsity pattern of the original matrix A. In particular, the product of terms C^T and C adds non-zero entries corresponding to DoF living on the interface only. Note that using a *discontinuous* space Λ_h for the Lagrange multiplier λ automatically gives a diagonal W.

2.3. Spectrum of the preconditioned matrix

We conduct numerical tests to evaluate the impact of the proposed preconditioner on the spectrum of $\mathcal{A}_\gamma$ (11). We consider the Poisson problem (2) with the following configuration:

- $\Omega = [0,1]^2$,
- $\omega = \mathcal{B}_r(\boldsymbol{c})$, where $\boldsymbol{c} = (0.5, 0.5)$ and $r = 0.21$.

We employ $\mathcal{Q}_1$ elements both for the background space V_h and the immersed space Λ_h. We consider four global refinements of the unit square, leading to $\mathsf{A} \in \mathbb{R}^{289\times289}$. The immersed mesh discretizing the interface consists of a uniform grid with 16 facets, so that $\mathsf{C} \in \mathbb{R}^{17\times289}$, giving a global block matrix $\mathcal{A}_\gamma \in \mathbb{R}^{306\times306}$. Above, $\mathcal{B}_r(\boldsymbol{c})$ denotes the ball of radius r centered at $\boldsymbol{c}$. We report in Fig. 2 the spectrum of both $\mathcal{A}_\gamma$ and $\mathcal{P}_\gamma^{-1}\mathcal{A}_\gamma$ matrices for different values of the parameter γ when using the *ideal* variant with $\mathsf{W} = \mathsf{M}_\lambda^2$. We point out that some of the eigenvalues of the original system are negative and close to zero, accordingly with the indefiniteness of the saddle point system. The strong clustering of the whole spectrum near one when the parameter γ increases is evident. This is consistent with the fact that $\gamma\mathsf{W}^{-1}$ increasingly provides a better approximation for the inverse of the Schur complement of $\mathcal{A}_\gamma$ as γ becomes larger. Notably, all the eigenvalues of the preconditioned system are positive and real.

3. Stokes fictitious domain problem

In this Section, we extend the AL-based preconditioner developed in Section 2.2 to the Stokes problem. We use bold letters to denote vector-valued functions, and we consider the following strong formulation:

$$\begin{cases} -\Delta \mathbf{u} + \nabla p = \mathbf{f} & \text{in } \Omega \setminus \Gamma, \\ \nabla \cdot \mathbf{u} = 0 & \text{in } \Omega \setminus \Gamma, \\ \mathbf{u} = \mathbf{g} & \text{on } \Gamma, \\ \mathbf{u} = \mathbf{0} & \text{on } \partial\Omega, \end{cases} \tag{18}$$

where $\mathbf{f} \in [L^2(\Omega)]^d$ and $\mathbf{g} \in [H^{\frac{1}{2}}(\Gamma)]^d$ are given data. The first two equations represent the classical Stokes problem, where $\mathbf{u}$ is a vector-valued function representing the velocity of the fluid, p a scalar function representing its pressure, and $\mathbf{f}$ are external body forces. The third equation imposes a constraint for the velocity field $\mathbf{u}$ on the immersed boundary Γ.
Concerning the incompressibility constraint, we observe that the boundary datum $\mathbf{g}$ must satisfy the following compatibility condition

$$\int_\Gamma \mathbf{g} \cdot \boldsymbol{n} = 0, \tag{19}$$

where $\boldsymbol{n}$ is the outward unit normal to Γ.
We now give the functional spaces for the continuous problem (18). For the velocity $\mathbf{u}$ we consider the usual choice

$$V(\Omega) := [H_0^1(\Omega)]^d = \{\mathbf{v} \in [H^1(\Omega)]^d : \mathbf{v}_{|\partial\Omega} = \mathbf{0}\}.$$

The pressure p naturally belongs to $L^2(\Omega)$ and is determined up to a constant that we fix such that p belongs to

$$Q(\Omega) := L_0^2(\Omega) = \left\{ q \in L^2(\Omega) : \int_\Omega q = 0 \right\}.$$

The functional space for the multiplier is chosen as

$$\Lambda(\Gamma) := [H^{-\frac{1}{2}}(\Gamma)]^d.$$

Problem (18) can be written as a constrained minimization problem by introducing the Lagrangian $\mathcal{L} : V(\Omega) \times Q(\Omega) \times \Lambda(\Gamma) \to \mathbb{R}$ defined as

$$\mathcal{L}(\mathbf{v}, q, \boldsymbol{\mu}) := \frac{1}{2}(\nabla \mathbf{v}, \nabla \mathbf{v})_\Omega - (\nabla \cdot \mathbf{v}, q)_\Omega - (\mathbf{f}, \mathbf{v})_\Omega + \langle \boldsymbol{\mu}, \mathbf{v} - \mathbf{g} \rangle_\Gamma. \tag{20}$$

Looking for stationary points of $\mathcal{L}$ gives the following *double* saddle point problem of finding $(\mathbf{u}, p, \boldsymbol{\lambda}) \in V(\Omega) \times Q(\Omega) \times \Lambda(\Gamma)$ such that

$$\begin{aligned} (\nabla \mathbf{v}, \nabla \mathbf{u})_\Omega - (\nabla \cdot \mathbf{v}, p)_\Omega + \langle \boldsymbol{\lambda}, \mathbf{v} \rangle_\Gamma &= (\mathbf{f}, \mathbf{v})_\Omega \qquad \forall \mathbf{v} \in V(\Omega), \\ (\nabla \cdot \mathbf{u}, q)_\Omega &= 0 \qquad \forall q \in Q(\Omega), \\ \langle \boldsymbol{\mu}, \mathbf{u} \rangle_\Gamma &= \langle \boldsymbol{\mu}, \mathbf{g} \rangle_\Gamma \qquad \forall \boldsymbol{\mu} \in \Lambda(\Gamma). \end{aligned} \tag{21}$$

In order to verify the well-posedness of the double saddle point problem above, we need to fulfill two inf-sup conditions (see [17]). The first inf-sup condition is the classical one for the Stokes problem.

Proposition 2. *There exists a constant $\beta_p > 0$ such that for all $q \in Q(\Omega)$*

$$\sup_{\mathbf{v} \in V(\Omega)} \frac{(\nabla \cdot \mathbf{v}, q)_\Omega}{\|\mathbf{v}\|_{1,\Omega}} \geq \beta_p ||q||_{0,\Omega}. \tag{22}$$

The second one is less standard and it is the inf-sup condition for the bilinear form $\langle \boldsymbol{\mu}, \mathbf{v} \rangle_\Gamma$ associated with the Lagrange multiplier $\boldsymbol{\lambda}$. Its precise statement follows as a particular case of the more general setting presented in [5] for the full fluid-structure interaction problem. Let us first set

$$K_0 := \{\mathbf{v} \in V(\Omega) : (\nabla \cdot \mathbf{v}, q)_\Omega = 0 \quad \forall q \in Q(\Omega)\} = \{\mathbf{v} \in V(\Omega) : \nabla \cdot \mathbf{v} = 0 \text{ in } \Omega\},$$

where the second equality follows upon testing against $q = \nabla \cdot \mathbf{v} \in Q(\Omega)$, since $\mathbf{v} \in \left[H_0^1(\Omega)\right]^d$.

Proposition 3 ([5], Proposition 13). *There exists a constant $\beta_\mu > 0$ such that for all $\boldsymbol{\mu} \in \Lambda(\Gamma)$ it holds*

$$\sup_{\mathbf{v} \in K_0} \frac{\langle \boldsymbol{\mu}, \mathbf{v} \rangle_\Gamma}{\|\mathbf{v}\|_{1,\Omega}} \geq \beta_\mu ||\boldsymbol{\mu}||_{-\frac{1}{2},\Gamma}. \tag{23}$$

Proof. Since $\Lambda(\Gamma) = [H^{-\frac{1}{2}}(\Gamma)]^d$, by definition of dual norm we have

$$||\boldsymbol{\mu}||_{-\frac{1}{2},\Gamma} = \sup_{\mathbf{z} \in H^{1/2}(\Gamma)} \frac{\langle \boldsymbol{\mu}, \mathbf{z} \rangle_\Gamma}{\|\mathbf{z}\|_{\frac{1}{2},\Gamma}}.$$

Let us now consider a maximizing sequence $\{\mathbf{z}_n\}_{n\in\mathbb{N}}$ such that

$$\lim_{n\to+\infty}\frac{\langle\boldsymbol{\mu},\mathbf{z}_n\rangle_\Gamma}{\|\mathbf{z}_n\|_{\frac{1}{2},\Gamma}}=\|\boldsymbol{\mu}\|_{-\frac{1}{2},\Gamma}.$$

Thanks to the surjectivity of the trace operator from $[H_0^1(\Omega)]^d$ to $[H^{1/2}(\Gamma)]^d$, it is possible to show (cfr. [5, Lemma 12]) the existence of $\mathbf{u}_n\in K_0$ such that $\mathbf{u}_{n|\Gamma}=\mathbf{z}_n$, with $\|\mathbf{u}_n\|_{1,\Omega}\le c\|\mathbf{z}_n\|_{\frac{1}{2},\Gamma}$. The desired inequality is then obtained as follows:

$$\sup_{\mathbf{v}\in K_0}\frac{\langle\boldsymbol{\mu},\mathbf{v}\rangle_\Gamma}{\|\mathbf{v}\|_{1,\Omega}}\ge\frac{\langle\boldsymbol{\mu},\mathbf{u}_n\rangle_\Gamma}{\|\mathbf{u}_n\|_{1,\Omega}}\ge\frac{1}{c}\frac{\langle\boldsymbol{\mu},\mathbf{z}_n\rangle_\Gamma}{\|\mathbf{z}_n\|_{\frac{1}{2},\Gamma}}\ge\frac{1}{2c}||\boldsymbol{\mu}||_{-\frac{1}{2},\Gamma},$$

where the last inequality follows from the fact that $\{\mathbf{z}_n\}_{n\in\mathbb{N}}$ is a maximizing sequence. □

Having these two inf-sup conditions, we can state a *combined inf-sup* condition involving $V(\Omega)$ and the graph space $M:=Q(\Omega)\times\Lambda(\Gamma)$ equipped with the natural norm $\|(q,\boldsymbol{\mu})\|_M^2:=\|q\|_{0,\Omega}^2+\|\boldsymbol{\mu}\|_{-\frac{1}{2},\Gamma}^2$, which will be needed in Section 4 for the spectral analysis of our preconditioner. This result is based on the abstract framework developed in [46] in the context of twofold saddle point problems, which we quote here in a simplified form for ease of exposition.

Theorem 2 ([46], Theorem 3.1). *Let U, P_1 and P_2 be reflexive Banach spaces, and let $b_1: U\times P_1\to\mathbb{R}$, and $b_2: U\times P_2\to\mathbb{R}$ be bilinear and continuous forms. Let*

$$Z_{b_1}:=\{v\in U:\ b_1(v,q_1)=0\quad\forall q_1\in P_1\}\subset U,$$

then the following conditions are equivalent:

1. *There exists $c>0$ such that*
$$\sup_{v\in U}\frac{b_1(v,p_1)+b_2(v,p_2)}{\|v\|_U}\ge c(\|p_1\|_{P_1}+\|p_2\|_{P_2})\qquad(p_1,p_2)\in P_1\times P_2.$$
2. *There exists $c>0$ such that*
$$\sup_{v\in U}\frac{b_1(v,p_1)}{\|v\|_U}\ge c\|p_1\|_{P_1},\quad p_1\in P_1$$
and
$$\sup_{v\in Z_{b_1}}\frac{b_2(v,p_2)}{\|v\|_U}\ge c\|p_2\|_{P_2},\quad p_2\in P_2.$$

We can therefore state the following combined inf-sup condition, which is a direct application of Propositions 2 and 3 above.

Proposition 4. *There exists a constant $C>0$ such that*

$$\sup_{\mathbf{v}\in V(\Omega)}\frac{(\nabla\cdot\mathbf{v},q)_\Omega+\langle\boldsymbol{\mu},\mathbf{v}\rangle_\Gamma}{\|\mathbf{v}\|_{1,\Omega}}\ge C\|(q,\boldsymbol{\mu})\|_M\qquad(q,\boldsymbol{\mu})\in M.\tag{24}$$

Proof. We set $U=V(\Omega)$, $P_1=Q(\Omega)$, and $P_2=\Lambda(\Gamma)$ in the statement of Theorem 2. As bilinear forms, it is sufficient to define $b_1(\mathbf{v},q):=(\nabla\cdot\mathbf{v},q)_\Omega$, and $b_2(\boldsymbol{\mu},\mathbf{v}):=\langle\boldsymbol{\mu},\mathbf{v}\rangle_\Gamma$. Finally, we define $Z_{b_1}=K_0$. Then, Theorem 2 implies that there exists a constant $C>0$ such that

$$\sup_{\mathbf{v}\in V(\Omega)}\frac{(\nabla\cdot\mathbf{v},q)_\Omega+\langle\boldsymbol{\mu},\mathbf{v}\rangle_\Gamma}{\|\mathbf{v}\|_{1,\Omega}}\ge C\Big(\|q\|_{0,\Omega}+\|\boldsymbol{\mu}\|_{-\frac{1}{2},\Gamma}\Big)\qquad(q,\boldsymbol{\mu})\in M.$$

The thesis follows using the fact that $\|q\|_{0,\Omega}+\|\boldsymbol{\mu}\|_{-\frac{1}{2},\Gamma}\ge\sqrt{\|q\|_{0,\Omega}^2+\|\boldsymbol{\mu}\|_{-\frac{1}{2},\Gamma}^2}=\|(q,\boldsymbol{\mu})\|_M$. □

3.1. Finite element discretization

We consider a finite element discretization based on mixed finite elements. In particular, we use the *stable* Taylor-Hood $\mathcal{Q}_2$-$\mathcal{Q}_1$ pair, i.e. continuous piecewise quadratic velocities and linear pressures [17]. We denote the associated finite-dimensional subspaces with $V_h\subset V(\Omega)$ and $Q_h\not\subset Q(\Omega)$ (we do not ask functions of Q_h to have zero average, therefore $Q_h\not\subset Q(\Omega)$). Analogously to the Poisson problem, we employ as a finite-dimensional subspace for the multiplier

$$\Lambda_h:=\{\boldsymbol{\mu}_h\in[L^2(\Gamma)]^d:\ \boldsymbol{\mu}_h|_K\in[\mathcal{Q}^1(K)]^d,\forall K\in\Gamma_h\}.\tag{25}$$

With these choices of finite element spaces, and denoting with $\{\boldsymbol{\varphi}_i\}_{i=1}^n$, $\{\phi_k\}_{k=1}^m$, and $\{\boldsymbol{\psi}_\alpha\}_{\alpha=1}^l$ the selected basis functions of V_h, Q_h, and Λ_h, we end up with the following linear system of equations for $(\mathrm{u},\mathrm{p},\lambda)$

$$\begin{bmatrix}\mathsf{A}&\mathsf{B}^\mathsf{T}&\mathsf{C}^\mathsf{T}\\ \mathsf{B}&0&0\\ \mathsf{C}&0&0\end{bmatrix}\begin{bmatrix}\mathrm{u}\\ \mathrm{p}\\ \lambda\end{bmatrix}=\begin{bmatrix}\mathrm{f}\\ 0\\ \mathrm{g}\end{bmatrix},\tag{26}$$

where

$$\begin{aligned} \mathsf{A}_{ij} &= (\nabla\boldsymbol{\varphi}_i, \nabla\boldsymbol{\varphi}_j)_\Omega \qquad i,j = 1,\dots,n \\ \mathsf{B}_{ki} &= -(\nabla\cdot\boldsymbol{\varphi}_i, \phi_k)_\Omega \qquad i = 1,\dots,n, \quad k = 1,\dots,m \\ \mathsf{C}_{\alpha i} &= \langle\boldsymbol{\varphi}_i, \boldsymbol{\psi}_\alpha\rangle_\Gamma \qquad i = 1,\dots,n, \quad \alpha = 1,\dots,l. \end{aligned}$$

As is customary in Immersed Boundary or Fictitious Domain methods, the velocity is fixed to 0 on the background boundary, i.e. $\mathbf{u}_{|\partial\Omega} = \mathbf{0}$. Due to this particular choice, the pressure field p is determined up to a constant. Choosing Q to be in $L^2_0(\Omega)$ fixes the uniqueness of the solution for the pressure in the continuous case, but not enforcing the zero average condition at the discrete level generates a matrix B which is not full row-rank and 0 is an eigenvalue of the system. To summarize, $\mathsf{A} \in \mathbb{R}^{n\times n}$ is symmetric positive definite, $\mathsf{B} \in \mathbb{R}^{m\times n}$ is rank deficient by 1 and $\mathsf{C} \in \mathbb{R}^{l\times n}$. As for the Poisson problem in Section 2, the fact that C is full row-rank is a consequence of the fulfillment of the inf-sup condition for the velocity-multiplier pair.
Sufficient conditions for the existence and uniqueness of the discrete problem are the discrete versions of the two inf-sup conditions for the continuous problem. Since the pair $V_h \times Q_h$ is stable, the discrete inf-sup condition for the Stokes problem is the standard discrete inf-sup condition for the divergence operator.

Proposition 5. *Let V_h and Q_h be defined as above, then there exists a positive constant β_1, independent of the mesh parameters, such that for all $q_h \in Q_h$ it holds*

$$\sup_{\mathbf{v}_h\in V_h} \frac{(\nabla\cdot\mathbf{v}_h, q_h)_\Omega}{\|\mathbf{v}_h\|_{1,\Omega}} \geq \beta_1 ||q_h||_{0,\Omega}. \tag{27}$$

The discrete analogue of Proposition 3, showing the inf-sup condition involving the discrete Lagrange multiplier, is a particular case of [5, Proposition 16]. We start by introducing the discrete version of the kernel K_0

$$K_{0,h} := \{\mathbf{v}_h \in V_h : (\nabla\cdot\mathbf{v}_h, q_h)_\Omega = 0 \quad \forall q_h \in Q_h\} \subset V_h.$$

Proposition 6 ([5], Proposition 16). *Let V_h, Q_h and Λ_h be defined as above. If h_Ω/h_Γ is sufficiently small and the mesh Γ_h is quasi-uniform, then there exists a constant $\beta_2 > 0$, independent of h_Ω and h_Γ, such that for all $\boldsymbol{\mu}_h \in \Lambda_h$ it holds*

$$\sup_{\mathbf{v}_h\in K_{0,h}} \frac{\langle\boldsymbol{\mu}_h, \mathbf{v}_h\rangle_\Gamma}{\|\mathbf{v}_h\|_{1,\Omega}} \geq \beta_2 ||\boldsymbol{\mu}_h||_{-\frac{1}{2},\Gamma}. \tag{28}$$

Remark 2. By definition, $K_{0,h} \subset V_h$. This allows us to rewrite the inf-sup condition in (28) on the whole V_h. More precisely, for all $\boldsymbol{\mu}_h \in \Lambda_h$ it holds

$$\beta_2 ||\boldsymbol{\mu}_h||_{-\frac{1}{2},\Gamma} \leq \sup_{\mathbf{v}_h\in K_{0,h}} \frac{\langle\boldsymbol{\mu}_h, \mathbf{v}_h\rangle_\Gamma}{\|\mathbf{v}_h\|_{1,\Omega}} \leq \sup_{\mathbf{v}_h\in V_h} \frac{\langle\boldsymbol{\mu}_h, \mathbf{v}_h\rangle_\Gamma}{\|\mathbf{v}_h\|_{1,\Omega}}. \tag{29}$$

Proceeding exactly as in the continuous case, we can exploit the two individual discrete inf-sup conditions (27) and (28), use Theorem 2, and obtain a combined inf-sup condition for the discrete case. We denote with $M_h := Q_h \times \Lambda_h$ the discrete version of the graph space M.

Proposition 7. *Let V_h, Q_h and Λ_h be defined as above. If h_Ω/h_Γ is sufficiently small and the mesh Γ_h is quasi-uniform, then there exists a constant $\beta_3 > 0$, independent of h_Ω and h_Γ, such that for all $(q_h, \boldsymbol{\mu}_h) \in M_h$ it holds*

$$\sup_{\mathbf{v}_h\in V_h} \frac{(\nabla\cdot\mathbf{v}_h, q_h)_\Omega + \langle\boldsymbol{\mu}_h, \mathbf{v}_h\rangle_\Gamma}{\|\mathbf{v}_h\|_{1,\Omega}} \geq \beta_3 \|(q_h, \boldsymbol{\mu}_h)\|_M. \tag{30}$$

Remark 3 (Finite element spaces)**.** Concerning the particular choice of the finite-dimensional subspaces, we notice that other choices are possible, such as $\mathcal{Q}_2$-$\mathcal{P}_1$, which use discontinuous piecewise linear pressures [47]. However, we stress that the forthcoming spectral analysis is generic and relies only on the choice of inf-sup stable elements.

3.2. Augmented Lagrangian preconditioner

Consider the $(n+m+l)\times(n+m+l)$ linear system of Eq. (26). To apply the same reasoning used for the Poisson case, we propose augmenting the (1,1)-block twice and reformulating the Stokes fictitious domain problem as the following equivalent system

$$\begin{bmatrix} \mathsf{A}+\gamma\mathsf{B}^\mathsf{T}\mathsf{Q}^{-1}\mathsf{B}+\delta\mathsf{C}^\mathsf{T}\mathsf{W}^{-1}\mathsf{C} & \mathsf{B}^\mathsf{T} & \mathsf{C}^\mathsf{T} \\ \mathsf{B} & 0 & 0 \\ \mathsf{C} & 0 & 0 \end{bmatrix} \begin{bmatrix} \mathsf{u} \\ \mathsf{p} \\ \lambda \end{bmatrix} = \begin{bmatrix} \mathsf{f}+\delta\mathsf{C}^\mathsf{T}\mathsf{W}^{-1}\mathsf{g} \\ 0 \\ \mathsf{g} \end{bmatrix} \quad \text{or} \quad \mathcal{A}_{\gamma\delta}\mathsf{x} = \hat{\mathsf{b}}. \tag{31}$$

Both Q and W are arbitrary SPD matrices and $\gamma > 0$, $\delta > 0$ are two real parameters to be selected. Then, we propose the following preconditioner:

$$\mathcal{P}_{\gamma\delta} = \begin{bmatrix} \mathsf{A}_{\gamma\delta} & \mathsf{B}^\mathsf{T} & \mathsf{C}^\mathsf{T} \\ 0 & -\frac{1}{\gamma}\mathsf{Q} & 0 \\ 0 & 0 & -\frac{1}{\delta}\mathsf{W} \end{bmatrix}, \tag{32}$$

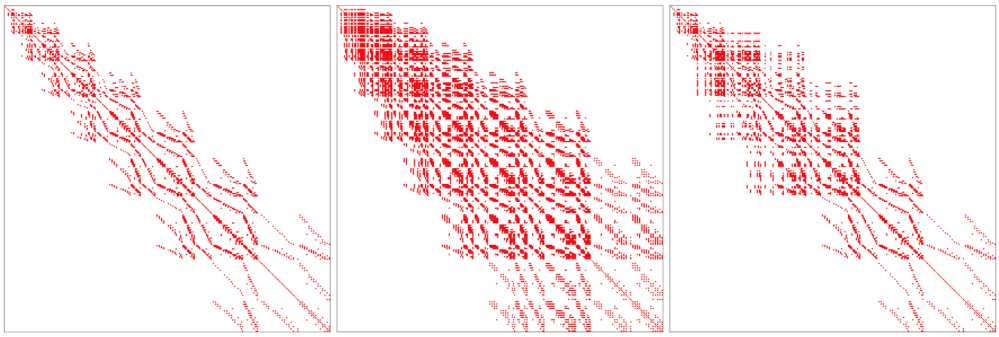

(a) A_{GD} NNZ: 12,228 (b) $A + B^T B$ NNZ: 40,168 (c) $A_{GD} + C^T C$ NNZ: 16,612

Fig. 3. Comparison of resulting sparsity patterns after different augmentations. Here we considered $A \in \mathbb{R}^{578\times578}$, $B \in \mathbb{R}^{81\times578}$, and $C \in \mathbb{R}^{34\times578}$. The resulting matrices stem from the discretization of the Stokes fictitious domain problem, using the configuration in Section 4.1. The matrix A_{GD} denotes the matrix A augmented with the Grad-Div stabilization.

which has inverse

$$\mathcal{P}_{\gamma\delta}^{-1} = \begin{bmatrix} A_{\gamma\delta}^{-1} & 0 & 0 \\ 0 & I_m & 0 \\ 0 & 0 & I_l \end{bmatrix} \begin{bmatrix} I_n & B^T & C^T \\ 0 & -I_m & 0 \\ 0 & 0 & -I_l \end{bmatrix} \begin{bmatrix} I_n & 0 & 0 \\ 0 & \gamma Q^{-1} & 0 \\ 0 & 0 & \delta W^{-1} \end{bmatrix}, \tag{33}$$

with $A_{\gamma\delta} := A + \gamma B^T Q^{-1} B + \delta C^T W^{-1} C$. It is well known [18] that for LBB-stable discretizations of the Stokes problem, if the Schur complement $S_B = BA^{-1}B^T$ is nonsingular, it is spectrally equivalent to the pressure mass matrix M_p. Otherwise, spectral equivalence holds on Ran(B), the range of B. We set $Q := M_p$. Motivated by its effectiveness in the scalar case investigated in Section (2) for the Poisson problem, we set again $W := M_\lambda^2$, defined analogously to the scalar case in (14) as

$$(M_\lambda)_{\alpha,\beta} := \int_\Gamma \boldsymbol{\psi}_\alpha \cdot \boldsymbol{\psi}_\beta \qquad \alpha, \beta = 1, \dots, l. \tag{34}$$

All in all, from Eq. (33) it is evident that the application of the proposed preconditioner $\mathcal{P}_{\gamma\delta}$ to a vector requires one solve with $A_{\gamma\delta}$, one with Q, and one with W, plus two sparse matrix-vector products. The considerations made for the scalar case in Section 2 also apply identically in this case. In particular, the overall complexity is shifted to the solution of the augmented velocity in the (1,1)-block.

Of course, one could think of avoiding assembling $A_{\gamma\delta}$ and instead use it as an operator, but this would prevent the usage of preconditioners such as AMG or ILU decompositions.

We first focus on the practical construction of $B^T Q^{-1} B$, which appears in the augmentation of the (1,1)-block. Note that if Q^{-1} is a dense matrix, then the product $B^T Q^{-1} B$ will also be dense. Furthermore, even when a diagonal approximation of Q is used, the product $B^T B$ may contain significantly more non-zero entries than A itself. A possible remedy to this issue is to use a *Grad-Div* stabilization. As discussed in [48], the *Grad-Div* stabilization can be interpreted as the sum of an algebraic term, given by $(B^T Q^{-1} B)_{ij}\ \forall i, j \in \{1, \dots, n\}$, and a projection-type stabilization term; see also [49]. This additional projection term vanishes asymptotically as the mesh is refined, making it reasonable to use the same AL approach to build the preconditioner, but without explicitly adding the augmentation to the (1,1)-block. Specifically, the contribution $\gamma\left(\nabla \cdot \boldsymbol{\varphi}_i, \nabla \cdot \boldsymbol{\varphi}_j\right)_{i,j}$ is directly added to the global matrix A during the assembly phase of the system, thus avoiding the issues related to the explicit computation of the product $B^T Q^{-1} B$. Replacing this augmentation by *Grad-Div* stabilization implies that new entries are added only where the components of the velocity couple. Fig. 3 illustrates the sparsity pattern of matrix A when *Grad-Div* stabilization is included (see Fig. 3a) and compares it to the sparsity pattern of the augmented matrix $A + B^T Q^{-1} B$ when A does not include the stabilization term, and Q is replaced with its main diagonal (see Fig. 3b).

On the other hand, we explicitly construct the term $C^T W^{-1} C$. When a diagonal approximation of W is used, as will be the case in Section 6.2, the influence of $C^T C$ on the sparsity pattern of the whole augmented block is minimal, especially compared to the influence of $B^T B$. This is clearly shown in Fig. 3c: the increase in the total number of non-zero entries in the final augmented block, where A includes the *Grad-Div* stabilization term, is much more favorable. In practice, we will experience the fill-in shown in Fig. 3c. Once the whole $A_{\gamma\delta}$ term is assembled, it is solved with CG preconditioned by a single V-cycle of AMG, using a very loose tolerance (such as 10^{-2}).

Remark 4 (Symmetric preconditioning)**.** The preconditioned system is non-symmetric since we are dealing with a block triangular preconditioner. Therefore, eigenvalue information alone is not sufficient to rigorously justify the mesh independence of the convergence of non-symmetric matrix iterations like GMRES [50]. For this reason, we have tested a symmetric and positive definite (block

diagonal) variant of our preconditioner, namely

$$\mathcal{P}_{\mathrm{sym},\gamma\delta} = \begin{bmatrix} \mathsf{A}_{\gamma\delta} & 0 & 0 \\ 0 & \frac{1}{\gamma}\mathsf{Q} & 0 \\ 0 & 0 & \frac{1}{\delta}\mathsf{W} \end{bmatrix}. \tag{35}$$

In fact, in this case, the preconditioned matrix is similar to a symmetric matrix, and the eigenvalues provide meaningful estimates of the convergence rate of a method like preconditioned MINRES. We note that while mesh independence is observed, the total number of outer iterations for the global system solved with MINRES preconditioned with the symmetric positive definite variant of $\mathcal{P}_{\gamma\delta}$ is higher than that obtained with FGMRES preconditioned by $\mathcal{P}_{\gamma\delta}$. In addition, note that the MINRES solver requires the preconditioner to be applied exactly (or iteratively but in an accurate way), meaning that the augmented block $\mathsf{A}_{\gamma\delta}$ needs to be solved with a stricter tolerance. This results in a high number of inner iterations. Hence, the block triangular preconditioner (32) outperforms the block diagonal one in terms of computational cost. Even if we lost the possible advantage of $\mathcal{A}_{\gamma\delta}$ being symmetric, using a method like FGMRES with block triangular preconditioning leads – in practice – to more rapid convergence.

4. Spectral analysis

In this Section, we derive lower and upper bounds for the eigenvalues of the preconditioned matrix $\mathcal{P}_{\gamma\delta}^{-1}\mathcal{A}_{\gamma\delta}$ for the Stokes problem. Although eigenvalue information alone is generally insufficient to predict the convergence behaviour of nonsymmetric Krylov subspace methods, practical experience suggests that convergence is often fast when the spectrum is real, positive, and confined within a moderately sized interval bounded away from 0. In the following, we denote with $\mathrm{Spec}(\mathsf{M})$ the spectrum of a generic square matrix M.

The next result, concerning the spectrum of the preconditioned matrix, is purely algebraic and does not depend on any physical interpretation of the matrices involved. In Section 4.2, we will refine this analysis for the particular case in which such matrices correspond to those arising from the Stokes fictitious domain formulation. In that case, it will be possible to prove that the eigenvalues of the preconditioned system are bounded away from zero uniformly in the discretization parameters.

Theorem 3. *Suppose that $\mathcal{A}_{\gamma\delta}$ and $\mathcal{P}_{\gamma\delta}$ are defined by the matrices in (31) and (32), respectively. The non-zero eigenvalues of $\mathcal{P}_{\gamma\delta}^{-1}\mathcal{A}_{\gamma\delta}$ are all real and positive. More precisely, let $(\mathsf{x};\mathsf{y};\mathsf{z})$ be an eigenvector of $\mathcal{P}_{\gamma\delta}^{-1}\mathcal{A}_{\gamma\delta}$, it holds*

$$\mathrm{Spec}(\mathcal{P}_{\gamma\delta}^{-1}\mathcal{A}_{\gamma\delta}) \subseteq [\min(\eta,\epsilon,\theta), 1],$$

where

$$\eta = \min\left\{ \frac{\gamma \mathsf{x}^{\mathsf{T}}\mathsf{B}^{\mathsf{T}}\mathsf{Q}^{-1}\mathsf{B}\mathsf{x}}{\mathsf{x}^{\mathsf{T}}(\mathsf{A}+\gamma\mathsf{B}^{\mathsf{T}}\mathsf{Q}^{-1}\mathsf{B})\mathsf{x}} \;\middle|\; \mathsf{x} \in \ker(\mathsf{C}) \setminus \ker(\mathsf{B}) \right\},$$

$$\epsilon = \min\left\{ \frac{\delta \mathsf{x}^{\mathsf{T}}\mathsf{C}^{\mathsf{T}}\mathsf{W}^{-1}\mathsf{C}\mathsf{x}}{\mathsf{x}^{\mathsf{T}}(\mathsf{A}+\delta\mathsf{C}^{\mathsf{T}}\mathsf{W}^{-1}\mathsf{C})\mathsf{x}} \;\middle|\; \mathsf{x} \in \ker(\mathsf{B}) \setminus \ker(\mathsf{C}) \right\},$$

$$\theta = \min\left\{ \frac{\mathsf{x}^{\mathsf{T}}(\gamma\mathsf{B}^{\mathsf{T}}\mathsf{Q}^{-1}\mathsf{B}+\delta\mathsf{C}^{\mathsf{T}}\mathsf{W}^{-1}\mathsf{C})\mathsf{x}}{\mathsf{x}^{\mathsf{T}}(\mathsf{A}+\gamma\mathsf{B}^{\mathsf{T}}\mathsf{Q}^{-1}\mathsf{B}+\delta\mathsf{C}^{\mathsf{T}}\mathsf{W}^{-1}\mathsf{C})\mathsf{x}} \;\middle|\; \mathsf{x} \notin \ker(\mathsf{B}) \cup \ker(\mathsf{C}) \right\},$$

and with $\lambda = 1$ being an eigenvalue of algebraic multiplicity at least n.

Proof. Let λ be an arbitrary eigenvalue of $\mathcal{P}_{\gamma\delta}^{-1}\mathcal{A}_{\gamma\delta}$ with a corresponding eigenvector $(\mathsf{x};\mathsf{y};\mathsf{z})$. The generalized eigenvalue problem can be written as

$$\begin{bmatrix} \mathsf{A}_{\gamma\delta} & \mathsf{B}^{\mathsf{T}} & \mathsf{C}^{\mathsf{T}} \\ \mathsf{B} & 0 & 0 \\ \mathsf{C} & 0 & 0 \end{bmatrix} \begin{bmatrix} \mathsf{x} \\ \mathsf{y} \\ \mathsf{z} \end{bmatrix} = \lambda \begin{bmatrix} \mathsf{A}_{\gamma\delta} & \mathsf{B}^{\mathsf{T}} & \mathsf{C}^{\mathsf{T}} \\ 0 & -\frac{1}{\gamma}\mathsf{Q} & 0 \\ 0 & 0 & -\frac{1}{\delta}\mathsf{W} \end{bmatrix} \begin{bmatrix} \mathsf{x} \\ \mathsf{y} \\ \mathsf{z} \end{bmatrix}, \tag{36}$$

which can be written explicitly as

$$\mathsf{A}_{\gamma\delta}\mathsf{x} + \mathsf{B}^{\mathsf{T}}\mathsf{y} + \mathsf{C}^{\mathsf{T}}\mathsf{z} = \lambda(\mathsf{A}_{\gamma\delta}\mathsf{x} + \mathsf{B}^{\mathsf{T}}\mathsf{y} + \mathsf{C}^{\mathsf{T}}\mathsf{z}), \tag{37}$$

$$\mathsf{B}\mathsf{x} = -\frac{\lambda}{\gamma}\mathsf{Q}\mathsf{y}, \tag{38}$$

$$\mathsf{C}\mathsf{x} = -\frac{\lambda}{\delta}\mathsf{W}\mathsf{z}. \tag{39}$$

Note that the zero eigenvalue of the matrix in (31) related to the rank deficiency of B does not affect the convergence of preconditioned GMRES and can be excluded from the discussion [18,40].

Notice that $\mathsf{x} \neq 0$; otherwise, in view of the fact that Q and W are SPD matrices, $\mathsf{x} = 0$ implies $(\mathsf{x};\mathsf{y};\mathsf{z}) = (0;0;0)$, in contradiction with the fact that $(\mathsf{x};\mathsf{y};\mathsf{z})$ is an eigenvector. Hence, from now on we assume that $\mathsf{x} \neq 0$.

It is clear from Eqs. (37)–(39) that $\lambda = 1$ is an eigenvalue of $\mathcal{P}_{\gamma\delta}^{-1}\mathcal{A}_{\gamma\delta}$ with the corresponding eigenvector $(x; -\gamma Q^{-1}Bx; -\delta W^{-1}Cx)$ when $x \notin \ker(B) \cup \ker(C)$. Obviously, $\lambda = 1$ is an eigenvalue associated also with the eigenvector $(x; 0; -\delta W^{-1}Cx)$ when $x \in \ker(B) \setminus \ker(C)$, with the eigenvector $(x; -\gamma Q^{-1}Bx; 0)$ when $x \in \ker(C) \setminus \ker(B)$ and with the eigenvector $(x; 0; 0)$ when $x \in \ker(B) \cap \ker(C)$. The algebraic multiplicity of this eigenvalue is therefore at least n.
From now on, we assume that $\lambda \neq 1$ (and $\lambda \neq 0$). From (37) we derive

$$A_{\gamma\delta}x + B^T y + C^T z = 0, \tag{40}$$

whereas from (38) and (39), we respectively obtain

$$y = -\frac{\gamma}{\lambda}Q^{-1}Bx \quad \text{and} \quad z = -\frac{\delta}{\lambda}W^{-1}Cx.$$

By substituting the preceding two relations in (40), it follows that

$$A_{\gamma\delta}x - \frac{\gamma}{\lambda}B^T Q^{-1}Bx - \frac{\delta}{\lambda}C^T W^{-1}Cx = 0. \tag{41}$$

Multiplying both sides of (41) by λx^*, we get

$$\lambda x^* A_{\gamma\delta}x - x^*(\gamma B^T Q^{-1}B + \delta C^T W^{-1}C)x = 0,$$

which is equivalent to

$$\lambda = \frac{x^*(\gamma B^T Q^{-1}B + \delta C^T W^{-1}C)x}{x^*(A + \gamma B^T Q^{-1}B + \delta C^T W^{-1}C)x}. \tag{42}$$

Taking into account that $\gamma B^T Q^{-1}B + \delta C^T W^{-1}C$ is the sum of two symmetric positive semidefinite matrices and A is SPD, we conclude that all the eigenvalues of $\mathcal{P}_{\gamma\delta}^{-1}\mathcal{A}_{\gamma\delta}$ are real.[1]
From (42) we also deduce that $\lambda < 1$, and that all eigenvalues satisfying (42) tend to 1 for γ and/or $\delta \to \infty$. Summarizing, we have the following cases:

- $x \in \ker(C) \setminus \ker(B)$,

  $$0 < \eta \leq \lambda = \frac{\gamma x^* B^T Q^{-1}Bx}{x^*(A + \gamma B^T Q^{-1}B)x} < 1,$$

  where

  $$\eta = \min\left\{ \frac{\gamma x^* B^T Q^{-1}Bx}{x^*(A + \gamma B^T Q^{-1}B)x} \;\middle|\; x \in \ker(C) \setminus \ker(B) \right\}.$$

- $x \in \ker(B) \setminus \ker(C)$,

  $$0 < \epsilon \leq \lambda = \frac{\delta x^* C^T W^{-1}Cx}{x^*(A + \delta C^T W^{-1}C)x} < 1,$$

  where

  $$\epsilon = \min\left\{ \frac{\delta x^* C^T W^{-1}Cx}{x^*(A + \delta C^T W^{-1}C)x} \;\middle|\; x \in \ker(B) \setminus \ker(C) \right\}.$$

- $x \notin \ker(B) \cup \ker(C)$,

  $$0 < \theta \leq \lambda = \frac{x^*(\gamma B^T Q^{-1}B + \delta C^T W^{-1}C)x}{x^*(A + \gamma B^T Q^{-1}B + \delta C^T W^{-1}C)x} < 1,$$

  where

  $$\theta = \min\left\{ \frac{x^*(\gamma B^T Q^{-1}B + \delta C^T W^{-1}C)x}{x^*(A + \gamma B^T Q^{-1}B + \delta C^T W^{-1}C)x} \;\middle|\; x \notin \ker(B) \cup \ker(C) \right\}.$$

It is easy to check that if $\lambda \neq 1$, then $x \in \ker(B) \cap \ker(C)$ implies $A_{\gamma\delta}x = 0$. Since $A_{\gamma\delta}$ is SPD, this means that x should be the zero vector, which is impossible. □

[1] Note that since λ is real, the corresponding eigenvector can also be chosen to be real and therefore x^* can be replaced by x^T.

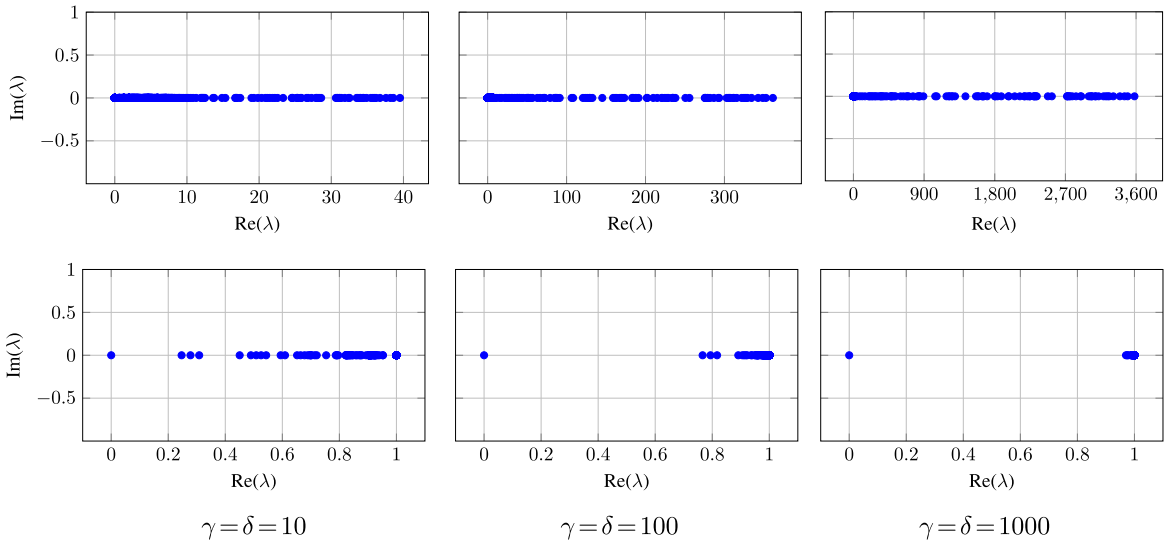

Fig. 4. Spectrum of the *original* system matrix $\mathcal{A}_{\gamma\delta}$ (top row) and $\mathcal{P}_{\gamma\delta}^{-1}\mathcal{A}_{\gamma\delta}$ (bottom row) for increasing values of γ and δ applied to the Stokes test case.

4.1. Spectrum of preconditioned matrix

We perform numerical tests to evaluate the theoretical findings in Theorem 3 and analyze the impact of the proposed preconditioner on the spectrum of the system in (31). We start with the following configuration for the Stokes problem:

- $\Omega = [0,1]^2$,
- $\omega = \mathcal{B}_r(\boldsymbol{c})$, where $\boldsymbol{c} = (0.45, 0.45)$ and $r = 0.21$.

We consider a discretization with $\mathcal{Q}_2$-$\mathcal{Q}_1$ elements for the velocity and pressure unknowns, while $\mathcal{Q}_1$ elements are used for the Lagrange multiplier. The background mesh consists of three uniform refinements of the unit square, while the immersed mesh consists of a uniform grid with 33 facets. For this discretization, we have $\mathsf{A} \in \mathbb{R}^{578\times578}$, the (negative) divergence matrix is $\mathsf{B} \in \mathbb{R}^{81\times578}$, and the coupling matrix is $\mathsf{C} \in \mathbb{R}^{34\times578}$, resulting in a global matrix $\mathcal{A}_{\gamma\delta} \in \mathbb{R}^{677\times677}$. The choices for Q and W are

- $\mathsf{Q} := \mathsf{M}_\mathsf{p}$ (pressure mass matrix),
- $\mathsf{W} := \mathsf{M}_\lambda^2$ (immersed mass matrix squared).

We report in Fig. 4 the spectrum of the unpreconditioned (top row) and preconditioned (bottom row) system matrix for increasing (but identical) values of the AL parameters δ and γ for the *ideal* preconditioner. We observe that, except for the zero eigenvalue, the rest of the eigenvalues are real and lie in the interval $(0, 1]$. Moreover, the non-zero eigenvalues of the preconditioned system are (incrementally) shifted towards 1 as the parameters δ and γ increase.

4.2. Mesh-independence for lower bound

Concerning the lower bound in Theorem 3, for suitable choices of the matrices Q and W it is possible to prove that λ is bounded away from zero uniformly in h_Ω and h_Γ, for all fixed γ and δ. We will first prove the result for $d = 2$, i.e. when Γ is a curve. The extension to the case $d = 3$ follows similarly and is given as a Remark at the end of this Section. Before delving into the proof, we collect some useful results we will need in the sequel. We start with the following inverse estimate, whose proof can be found in Appendix B.

Lemma 1. *Let Λ_h be the space for the discrete Lagrange multiplier, defined in (25). Then, there exists a constant $C > 0$ independent of the mesh size h_Γ such that the following estimate holds:*

$$||\mu_h||_{-\frac{1}{2},\Gamma} \geq C h_\Gamma^{\frac{1}{2}} ||\mu_h||_{0,\Gamma} \qquad \forall \mu_h \in \Lambda_h. \tag{43}$$

Using Lemma (1) above, we get the following alternative characterization of the discrete inf-sup condition (29).

Proposition 8. *Let V_h and Λ_h be defined as in Section 3.1. If h_Ω/h_Γ is sufficiently small and the mesh Γ_h is quasi-uniform, then there exists a positive constant $\tilde{\beta}_2$ independent of the mesh sizes h_Ω and h_Γ such that the following rescaled inf-sup condition holds*

$$\inf_{\mu_h\in\Lambda_h} \sup_{v_h\in V_h} \frac{\langle \mu_h, v_h\rangle_\Gamma}{||\mu_h||_{0,\Gamma}\,||v_h||_{1,\Omega}} \geq h_\Gamma^{-\frac{1}{2}} \tilde{\beta}_2. \tag{44}$$

Alternative equivalence results between scaled norm and $H^{\frac{1}{2}}$ norms have been shown through localization techniques in [51] and recently extended to the $H^{-\frac{1}{2}}$ case by Bertoluzza in [52].
In addition, we report the following well-known result concerning the general theory of the generalized Rayleigh quotient, which will be useful in what follows.

Remark 5. Let M and N be symmetric and symmetric positive definite matrices, respectively, with generalized eigenvalues $\lambda_1 \leq \ldots \leq \lambda_n$ and eigenvectors $\mathsf{v}_1, \ldots, \mathsf{v}_n \in \mathbb{R}^n$, such that $\mathsf{M}\mathsf{v}_i = \lambda_i \mathsf{N}\mathsf{v}_i$. Let $\mathsf{x} \in \mathbb{R}^n$, denote an arbitrary vector. Then:

- The smallest eigenvalue λ_1 can be characterized as

$$\lambda_1 = \min_{\mathsf{x}\neq 0} \frac{\mathsf{x}^\mathsf{T}\mathsf{M}\mathsf{x}}{\mathsf{x}^\mathsf{T}\mathsf{N}\mathsf{x}}, \quad \text{achieved when } \mathsf{x} = \pm \mathsf{v}_1.$$

- The second smallest eigenvalue λ_2 satisfies

$$\lambda_2 = \min_{\substack{\mathsf{x}\neq 0 \\ \mathsf{x}^\mathsf{T}\mathsf{N}\mathsf{v}_1 = 0}} \frac{\mathsf{x}^\mathsf{T}\mathsf{M}\mathsf{x}}{\mathsf{x}^\mathsf{T}\mathsf{N}\mathsf{x}}, \quad \text{achieved when } \mathsf{x} = \pm \mathsf{v}_2,$$

and so on.

Finally, norms of finite element functions can be computed using the following definitions:

$$|v_h|_{1,\Omega} = (\mathsf{v}^\mathsf{T}\mathsf{A}\mathsf{v})^{1/2}, \tag{45}$$

$$\|\mu_h\|_{0,\Gamma} = (\mu^\mathsf{T}\mathsf{M}_\lambda\mu)^{1/2}, \tag{46}$$

$$\|q_h\|_{0,\Omega} = (\mathsf{q}^\mathsf{T}\mathsf{M}_\mathsf{p}\mathsf{q})^{1/2}, \tag{47}$$

where v, q and μ are vectors of the coefficients associated with the velocity, pressure and Lagrange multiplier basis functions, and $\mathsf{A}, \mathsf{M}_\mathsf{p}, \mathsf{M}_\lambda$ are the usual stiffness and mass matrices. To prove mesh-independence for the lower bound of the preconditioned system, we will link the discrete inf-sup conditions to suitable generalized eigenvalue problems. The following three lemmas provide an algebraic interpretation of the discrete inf-sup stability conditions presented in Section 3.

Lemma 2. *Let A, B, and M_p be the matrices defined in Section 3, and assume that the discrete inf-sup condition in Proposition 5 is satisfied. Then, the inf-sup constant $\beta_1 > 0$ is such that*

$$\beta_1^2 = \min_{\{\mathsf{v}\in\mathbb{R}^n \,|\, \mathsf{u}^\mathsf{T}\mathsf{A}\mathsf{v}=0 \text{ for } \mathsf{u}\in\ker(\mathsf{B})\}} \frac{\mathsf{v}^\mathsf{T}\mathsf{B}^\mathsf{T}\mathsf{M}_\mathsf{p}^{-1}\mathsf{B}\mathsf{v}}{\mathsf{v}^\mathsf{T}\mathsf{A}\mathsf{v}}. \tag{48}$$

Proof. A proof of this result can be found in [18] (p. 193), or in [53], where the classical Stokes problem is analyzed in detail. Notice that the matrices A, B and M_p are exactly those of the classical Stokes problem defined in Ω, without an immersed boundary. □

Lemma 3. *Let A, C, and M_λ be the matrices defined in Section 3, and assume that the discrete inf-sup condition (29) is satisfied. Then, there exists a positive constant $\tilde{\beta}_2$ independent of h_Γ, such that*

$$\tilde{\beta}_2^2 \leq \min_{\{\mathsf{v}\in\mathbb{R}^n \,|\, \mathsf{u}^\mathsf{T}\mathsf{A}\mathsf{v}=0 \text{ for } \mathsf{u}\in\ker(\mathsf{C})\}} \frac{\mathsf{v}^\mathsf{T}\mathsf{C}^\mathsf{T}\mathsf{M}_\lambda^{-2}\mathsf{C}\mathsf{v}}{\mathsf{v}^\mathsf{T}\mathsf{A}\mathsf{v}}. \tag{49}$$

Proof. Using the matrix norms (45), (46) and given that $\langle \mu_h, v_h \rangle_\Gamma = \mathsf{v}^\mathsf{T}\mathsf{C}^\mathsf{T}\mu$, it is possible to give an algebraic interpretation of the discrete inf-sup stability condition in Proposition 8. In particular we have:

$$\inf_{\mu} \sup_{\mathsf{v}} \frac{\mathsf{v}^\mathsf{T}\mathsf{C}^\mathsf{T}\mu}{(\mathsf{v}^\mathsf{T}\mathsf{A}\mathsf{v})^{\frac{1}{2}} (\mu^\mathsf{T} h_\Gamma \mathsf{M}_\lambda \mu)^{\frac{1}{2}}} \geq \tilde{\beta}_2. \tag{50}$$

Arguing as in [53], let $0 < \sigma_1 \leq \sigma_2 \leq \ldots \leq \sigma_l$ be the l largest generalized eigenvalues of

$$\mathsf{C}^\mathsf{T} h_\Gamma^{-1} \mathsf{M}_\lambda^{-1} \mathsf{C}\mathsf{v} = \sigma \mathsf{A}\mathsf{v}. \tag{51}$$

Therefore, the constant appearing in the inf-sup condition (44) is given by the square root of σ_1, which is hence independent of the mesh size (this result can be proved following the same approach used in [53], where the classical Stokes problem is considered).
In other words, considering Remark 5 and given the fact that $\mathsf{C}^\mathsf{T} h_\Gamma^{-1} \mathsf{M}_\lambda^{-1} \mathsf{C}$ is a symmetric and positive semidefinite matrix, the following characterization holds:

$$\tilde{\beta}_2^2 = \sigma_1 = \min_{\{\mathsf{v}\in\mathbb{R}^n \,|\, \mathsf{u}^\mathsf{T}\mathsf{A}\mathsf{v}=0 \text{ for } \mathsf{u}\in\ker(\mathsf{C})\}} \frac{\mathsf{v}^\mathsf{T}\mathsf{C}^\mathsf{T} h_\Gamma^{-1} \mathsf{M}_\lambda^{-1} \mathsf{C}\mathsf{v}}{\mathsf{v}^\mathsf{T}\mathsf{A}\mathsf{v}}. \tag{52}$$

Furthermore, for a one-dimensional immersed domain embedded in a two-dimensional background domain, it can be shown that $(h_\Gamma \mathsf{M}_\lambda)^{-1}$ and M_λ^{-2} are spectrally equivalent, i.e.

$$0 < \frac{c}{C^2} \leq \frac{\mu^\mathsf{T}\mathsf{M}_\lambda^{-2}\mu}{\mu^\mathsf{T}(h_\Gamma \mathsf{M}_\lambda)^{-1}\mu} \leq \frac{C}{c^2}, \tag{53}$$

for some positive constants c, C independent of the discretization parameters (the details can be found in Appendix A). Setting $\mu = Cv$, and multiplying each term of (53) by $\frac{\mu^T (h_\Gamma M_\lambda)^{-1} \mu}{v^T A v}$, we get

$$0 < \frac{c}{C^2} \frac{v^T C^T (h_\Gamma M_\lambda)^{-1} C v}{v^T A v} \leq \frac{v^T C^T M_\lambda^{-2} C v,}{v^T A v} \leq \frac{C}{c^2} \frac{v^T C^T (h_\Gamma M_\lambda)^{-1} C v}{v^T A v}.$$

Combining this result with (52), it follows that

$$\tilde{\beta}_2^2 \leq \min_{\{v \in \mathbb{R}^n | u^T A v = 0 \text{ for } u \in \ker(C)\}} \frac{v^T C^T M_\lambda^{-2} C v}{v^T A v} \tag{54}$$

(where $\tilde{\beta}_2^2 := \frac{c}{C^2} \sigma_1$), uniformly in h_Γ. □

Lemma 4. *Let A, B, C, M_p and M_λ be the matrices defined in Section 3, and assume that the two inf-sup conditions (27) and (29) are satisfied. Then, there exists a positive constant $\tilde{\beta}_3 > 0$ independent of both h_Ω and h_Γ, such that*

$$\tilde{\beta}_3^2 \leq \min_{\{v \in \mathbb{R}^n | u^T A v = 0 \text{ for } u \in \ker(C) \cap \ker(B)\}} \frac{v^T (B^T M_p^{-1} B + C^T M_\lambda^{-2} C) v}{v^T A v}. \tag{55}$$

Proof. The discrete counterpart of the original double saddle point problem (21) can be equivalently rewritten as

$$\begin{aligned} (\nabla \mathbf{v}_h, \nabla \mathbf{u}_h)_\Omega - (\nabla \cdot \mathbf{v}_h, p_h)_\Omega + \langle \boldsymbol{\lambda}_h, \mathbf{v}_h \rangle_\Gamma &= (\mathbf{f}, \mathbf{v}_h)_\Omega \qquad \forall \mathbf{v}_h \in V_h, \\ -(\nabla \cdot \mathbf{u}_h, q_h)_\Omega + \langle \boldsymbol{\mu}_h, \mathbf{u}_h \rangle_\Gamma &= \langle \boldsymbol{\mu}_h, \mathbf{g} \rangle_\Gamma \qquad \forall (q_h, \boldsymbol{\mu}_h) \in M_h. \end{aligned} \tag{56}$$

Problem (56) is associated with the following partition of the original saddle point matrix

$$\begin{bmatrix} A & B^T & C^T \\ B & 0 & 0 \\ C & 0 & 0 \end{bmatrix} = \begin{bmatrix} A & D^T \\ D & 0 \end{bmatrix}, \tag{57}$$

where $D := \begin{bmatrix} B \\ C \end{bmatrix}$. Defining the bilinear form $d : V \times M \to \mathbb{R}$ as $d(\mathbf{v}, (q, \boldsymbol{\mu})) = (\nabla \cdot \mathbf{v}, q)_\Omega + \langle \boldsymbol{\mu}, \mathbf{v} \rangle_\Gamma$, we have that at the discrete level $d(\cdot, \cdot)$ can be evaluated as

$$d(\mathbf{v}_h, (q_h, \boldsymbol{\mu}_h)) = v^T B^T q + v^T C^T \mu.$$

Using now the matrix norms (45), (46), (47), and the definition of the norm

$$||(\boldsymbol{\mu}_h, q_h)||_M^2 = ||q_h||_Q^2 + ||\boldsymbol{\mu}_h||_\Lambda^2,$$

it is possible to give an algebraic interpretation of the discrete inf-sup stability condition in Proposition 7, using the rescaled variant provided by Lemma 1. In particular, we have:

$$\inf_{(\mu,q)} \sup_{v} \frac{v^T B^T q + v^T C^T \mu}{(v^T A v)^{\frac{1}{2}} (q^T M_p q + \mu^T h_\Gamma M_\lambda \mu)^{\frac{1}{2}}} \geq \tilde{\beta}_3. \tag{58}$$

Arguing again as in [53], let $0 < \sigma_1 \leq \sigma_2 \leq \dots$ be the nonzero generalized eigenvalues of

$$(B^T M_p^{-1} B + C^T h_\Gamma^{-1} M_\lambda^{-1} C) v = \sigma A v. \tag{59}$$

Then, the constant appearing in the inf-sup condition (58) is given by the square root of σ_1, which is therefore independent of the mesh size. Then, considering the properties of the generalized Rayleigh quotient, the following characterization holds:

$$\tilde{\beta}_3^2 = \sigma_1 = \min_{\{v \in \mathbb{R}^n | u^T A v = 0 \text{ for } u \in \ker(B) \cap \ker(C)\}} \frac{v^T B^T M_p^{-1} B v + v^T C^T h_\Gamma^{-1} M_\lambda^{-1} C v}{v^T A v}. \tag{60}$$

Furthermore, using the spectral equivalence between $(h_\Gamma M_\lambda)^{-1}$ and M_λ^{-2} as in the previous case, we can conclude that

$$\tilde{\beta}_3^2 \leq \min_{\{v \in \mathbb{R}^n | u^T A v = 0 \text{ for } u \in \ker(B) \cap \ker(C)\}} \frac{v^T B^T M_p^{-1} B v + v^T C^T M_\lambda^{-2} C v}{v^T A v}. \tag{61}$$

□

Theorem 4. *Let V_h, Q_h and Λ_h be defined as in Section 3.1. If $Q := M_p$, and $W := M_\lambda^2$, then the lower bound in*

$$\mathrm{Spec}(\mathcal{P}_{\gamma\delta}^{-1} \mathcal{A}_{\gamma\delta}) \subseteq [\min(\eta, \epsilon, \theta), 1]$$

from Theorem 3 is bounded away from zero by a positive constant independent of the discretization parameters h_Ω and h_Γ.

Proof. From the proof of Theorem 3 (more precisely from Eq. (41)), we know that all eigenvalues of $\mathcal{P}_{\gamma\delta}^{-1}\mathcal{A}_{\gamma\delta}$, except for those that are equal to 0 and 1, coincide with the eigenvalues of the following generalized eigenvalue problem:

$$(\gamma B^T Q^{-1} B + \delta C^T W^{-1} C)x = \lambda(A + \gamma B^T Q^{-1} B + \delta C^T W^{-1} C)x, \tag{62}$$

and they are all real. Therefore, the corresponding eigenvector can also be chosen to be real and, from now on, x^* is replaced by x^T. Our goal is to show that $\lambda^+_{\min}$, the smallest positive eigenvalue of (62), is bounded away from zero. To this end, we analyze separately the three cases considered in Theorem 3.

- $x \in \ker(C) \setminus \ker(B)$. We want to estimate η. From Theorem 3, we know that

$$\eta \le \lambda = \frac{\gamma x^T B^T M_p^{-1} B x}{x^T (A + \gamma B^T M_p^{-1} B)x}. \tag{63}$$

  Therefore, η coincides with the smallest positive eigenvalue of the generalized eigenvalue problem

$$\gamma B^T M_p^{-1} B x = \lambda(A + \gamma B^T M_p^{-1} B)x.$$

  In other words,

$$\eta = \min_{v \in \mathcal{R}} \frac{\gamma v^T B^T M_p^{-1} B v}{v^T (A + \gamma B^T M_p^{-1} B)v},$$

  where $\mathcal{R}$ is defined as

$$\mathcal{R} := \{v \in \mathbb{R}^n | u^T (A + \gamma B^T M_p^{-1} B)v = 0 \quad \forall u \in \ker(B)\}.$$

  Since $u \in \ker(B)$, it follows that the condition in $\mathcal{R}$ reduces to

$$u^T A v = 0 \quad \forall u \in \ker(B),$$

  and thus we can equivalently define

$$\mathcal{R} := \{v \in \mathbb{R}^n | u^T A v = 0 \quad \forall u \in \ker(B)\}.$$

  Next, we multiply and then divide by $v^T A v$ to obtain

$$\eta = \min_{v \in \mathcal{R}} \frac{\gamma v^T B^T M_p^{-1} B v}{v^T A v} \frac{v^T A v}{v^T A v + \gamma v^T B^T M_p^{-1} B v}.$$

  Let $r(v) := \frac{v^T B^T M_p^{-1} B v}{v^T A v}$ be the generalized Rayleigh quotient associated with $B^T M_p^{-1} B$ and A. Then we observe that η can be written as

$$\eta = \min_{v \in \mathcal{R}} \frac{\gamma r(v)}{1 + \gamma r(v)} = \min_{v \in \mathcal{R}} f(r(v)).$$

  Since $f(r(v)) = \frac{\gamma r(v)}{1+\gamma r(v)}$ is a monotone increasing function for $r(v) > 0$,

$$\min_{v \in \mathcal{R}} f(r(v)) = f(\min_{v \in \mathcal{R}} r(v)).$$

  From Lemma (2) we have $\min_{v \in \mathcal{R}} r(v) = \beta_1^2$, therefore we can conclude that

$$\eta = f(\beta_1^2) = \frac{\gamma \beta_1^2}{1 + \gamma \beta_1^2} > 0, \tag{64}$$

  uniformly in h_Ω, which completes the estimate for η.

- $x \in \ker(B) \setminus \ker(C)$. From Theorem 3, we know that

$$\epsilon \le \lambda = \frac{\delta x^T C^T M_\lambda^{-2} C x}{x^T (A + \delta C^T M_\lambda^{-2} C)x}. \tag{65}$$

  Arguing as in the previous case, ϵ can be written as

$$\epsilon = \min_{v \in \mathcal{R}} \frac{\delta v^T C^T M_\lambda^{-2} C v}{v^T (A + \delta C^T M_\lambda^{-2} C)v},$$

  where, to keep the notation simple, we will again denote by $\mathcal{R}$ the set of vectors v that are A-orthogonal to $\ker(C)$.
  We multiply and then divide by $v^T A v$ to obtain

$$\epsilon = \min_{v \in \mathcal{R}} \frac{\delta v^T C^T M_\lambda^{-2} C v}{v^T A v} \frac{v^T A v}{v^T A v + \delta v^T C^T M_\lambda^{-2} C v}.$$

Once again, we define the generalized Rayleigh quotient $r(\mathsf{v}) := \frac{\mathsf{v}^\mathsf{T}\mathsf{C}^\mathsf{T}\mathsf{M}_\lambda^{-2}\mathsf{C}\mathsf{v}}{\mathsf{v}^\mathsf{T}\mathsf{A}\mathsf{v}}$, so that ϵ can be written as

$$\epsilon = \min_{\mathsf{v}\in\mathcal{R}} \frac{\delta r(\mathsf{v})}{1+\delta r(\mathsf{v})} = \min_{\mathsf{v}\in\mathcal{R}} f(r(\mathsf{v})),$$

where $f(r(\mathsf{v}))$ is a monotone increasing function for $r(\mathsf{v}) > 0$. Therefore, we need to characterize $f(\min_{\mathsf{v}\in\mathcal{R}} r(\mathsf{v}))$. To this aim, we use Lemma 3, from which we know that $\min_{\mathsf{v}\in\mathcal{R}} r(\mathsf{v}) \geq \tilde{\beta}_2^2$, therefore it follows that

$$\epsilon \geq f(\tilde{\beta}_2^2) = \frac{\delta\tilde{\beta}_2^2}{1+\delta\tilde{\beta}_2^2} > 0, \tag{66}$$

uniformly in h_Γ.

Remark 6. We emphasize that this result, derived in the context of the Stokes fictitious domain problem, also applies to the Poisson fictitious domain problem. In particular, it shows that the eigenvalues of the preconditioned matrix remain uniformly bounded away from zero also for the Poisson problem.

- $\mathsf{x} \notin \ker(\mathsf{B}) \cup \ker(\mathsf{C})$. From Theorem 3, we know that

$$\theta \leq \lambda = \frac{\mathsf{x}^\mathsf{T}\left(\gamma\,\mathsf{B}^\mathsf{T}\mathsf{M}_\mathsf{p}^{-1}\mathsf{B} + \delta\,\mathsf{C}^\mathsf{T}\mathsf{M}_\lambda^{-2}\mathsf{C}\right)\mathsf{x}}{\mathsf{x}^\mathsf{T}\left(\mathsf{A} + \gamma\,\mathsf{B}^\mathsf{T}\mathsf{M}_\mathsf{p}^{-1}\mathsf{B} + \delta\,\mathsf{C}^\mathsf{T}\mathsf{M}_\lambda^{-2}\mathsf{C}\right)\mathsf{x}}.$$

As in the previous cases, we have

$$\theta = \min_{\mathsf{v}\in\mathcal{R}} \frac{\mathsf{v}^\mathsf{T}\left(\gamma\,\mathsf{B}^\mathsf{T}\mathsf{M}_\mathsf{p}^{-1}\mathsf{B} + \delta\,\mathsf{C}^\mathsf{T}\mathsf{M}_\lambda^{-2}\mathsf{C}\right)\mathsf{v}}{\mathsf{v}^\mathsf{T}\left(\mathsf{A} + \gamma\,\mathsf{B}^\mathsf{T}\mathsf{M}_\mathsf{p}^{-1}\mathsf{B} + \delta\,\mathsf{C}^\mathsf{T}\mathsf{M}_\lambda^{-2}\mathsf{C}\right)\mathsf{v}},$$

where now

$$\mathcal{R} := \left\{\mathsf{v}\in\mathbb{R}^n \,\middle|\, \mathsf{u}^\mathsf{T}\mathsf{A}\mathsf{v} = 0 \quad \forall \mathsf{u}\in\ker(\mathsf{B})\cap\ker(\mathsf{C})\right\}.$$

Proceeding as before, we multiply and divide by $\mathsf{v}^\mathsf{T}\mathsf{A}\mathsf{v}$, and define the generalized Rayleigh quotient

$$r(\mathsf{v}) := \frac{\mathsf{v}^\mathsf{T}\left(\mathsf{B}^\mathsf{T}\mathsf{M}_\mathsf{p}^{-1}\mathsf{B} + \mathsf{C}^\mathsf{T}\mathsf{M}_\lambda^{-2}\mathsf{C}\right)\mathsf{v}}{\mathsf{v}^\mathsf{T}\mathsf{A}\mathsf{v}}.$$

It follows that

$$\theta \geq f\left(\min\{\gamma,\delta\}\ \min_{\mathsf{v}\in\mathcal{R}} r(\mathsf{v})\right),$$

where $f(\cdot)$ is defined analogously as before. Owing to Lemma 4, we know that $\min_{\mathsf{v}\in\mathcal{R}} r(\mathsf{v}) \geq \tilde{\beta}_3^2$, which in turn implies

$$\theta \geq f\left(\min\{\gamma,\delta\}\ \tilde{\beta}_3^2\right) = \frac{\min\{\gamma,\delta\}\ \tilde{\beta}_3^2}{1+\min\{\gamma,\delta\}\ \tilde{\beta}_3^2} > 0, \tag{67}$$

uniformly in h_Ω and h_Γ.

□

Remark 7 (Three-dimensional case)**.** When $\Omega\subset\mathbb{R}^3$, the immersed domain Γ is discretized with a surface mesh Γ_h. Assuming a quasi-uniform discretization for Γ_h, it holds

$$ch_\Gamma^2 \leq \frac{\mu^\mathsf{T}\mathsf{M}_\lambda\mu}{\mu^\mathsf{T}\mu} \leq Ch_\Gamma^2 \qquad \forall\mu\in\mathbb{R}^l, \tag{68}$$

yielding (see also Appendix A)

$$0 < \frac{c}{C^2h_\Gamma} \leq \frac{\mu^\mathsf{T}\mathsf{M}_\lambda^{-2}\mu}{\mu^\mathsf{T}(h_\Gamma\mathsf{M}_\lambda)^{-1}\mu} \leq \frac{C}{c^2h_\Gamma}. \tag{69}$$

Setting again $\mu = C\mathsf{v}$ in the proof of Lemma 3, it holds that

$$\min_{\{\mathsf{v}\in\mathbb{R}^n|\mathsf{u}^\mathsf{T}\mathsf{A}\mathsf{v}=0 \text{ for } \mathsf{u}\in\ker(\mathsf{C})\}} \frac{\mathsf{v}^\mathsf{T}\mathsf{C}^\mathsf{T}\mathsf{M}_\lambda^{-2}\mathsf{C}\mathsf{v}}{\mathsf{v}^\mathsf{T}\mathsf{A}\mathsf{v}} \geq \frac{\tilde{\beta}_2^2}{h_\Gamma}. \tag{70}$$

Following the same steps used to derive Eq. (66), we employ the inequality in (70) above to obtain

$$0 < \frac{\delta\tilde{\beta}_2^2}{h_\Gamma+\delta\tilde{\beta}_2^2} \leq \epsilon \qquad \text{for } \mathsf{x}\in\ker(\mathsf{B})\setminus\ker(\mathsf{C}). \tag{71}$$

By repeating the same reasoning but starting from Lemma 4, and simply adapting Eq. (60), we get

$$0 < \frac{\min\{\gamma,\delta\}\ \tilde{\beta}_3^2}{\max\left\{1, \frac{C^2 h_\Gamma}{c}\right\} + \min\{\gamma,\delta\}\ \tilde{\beta}_3^2} \le \theta \qquad \text{for } \mathsf{x} \notin \ker(\mathsf{B}) \cup \ker(\mathsf{C}). \tag{72}$$

Notice how in these cases the lower bound for the eigenvalues of the preconditioned matrix depends explicitly on h_Γ. However, it is immediate to observe that as $h_\Gamma \to 0$, the lower bound in (71) tends to 1, and also (72) remains bounded away from zero. Therefore, we can still conclude that also in this scenario the bounds are robust with respect to the discretization parameters.

5. Spectral analysis of the inexact variant of $\mathcal{P}_{\gamma\delta}$

In this Section, we discuss in detail the eigenvalue distribution of the preconditioned matrix when an inexact version of the proposed AL-based preconditioner (32) is employed. We mainly follow the analysis presented in [28]. For the sake of readability, we now drop γ, δ and write $\bar{\mathsf{A}}$ in place of $\mathsf{A}_{\gamma\delta}$ and P in place of $\mathcal{P}_{\gamma\delta}$, so that our *ideal* preconditioner reads

$$\mathsf{P} = \begin{bmatrix} \bar{\mathsf{A}} & \mathsf{B}^\mathsf{T} & \mathsf{C}^\mathsf{T} \\ 0 & -\frac{1}{\gamma}\mathsf{Q} & 0 \\ 0 & 0 & -\frac{1}{\delta}\mathsf{W} \end{bmatrix}. \tag{73}$$

In order to use the same notation as in [28], we define

$$\mathsf{S} := \frac{1}{\gamma}\mathsf{Q} \qquad \text{and} \qquad \mathsf{X} := \frac{1}{\delta}\mathsf{W}.$$

Due to the expensive solve associated in particular with the (1,1)-block, the ideal preconditioner P is not practical and needs to be replaced by an approximation. In practice, we will employ approximations also for the matrices Q and W. Hence, we are to analyze the following inexact version:

$$\bar{\mathsf{P}} := \begin{bmatrix} \hat{\mathsf{A}} & \mathsf{B}^\mathsf{T} & \mathsf{C}^\mathsf{T} \\ 0 & -\hat{\mathsf{S}} & 0 \\ 0 & 0 & -\hat{\mathsf{X}} \end{bmatrix},$$

where $\hat{\mathsf{A}}$, $\hat{\mathsf{S}}$, and $\hat{\mathsf{X}}$ represent symmetric positive definite approximations of $\bar{\mathsf{A}}$, S, and X, respectively. The spectral properties of the preconditioned matrix will be given in terms of the eigenvalues of $\hat{\mathsf{A}}^{-1}\bar{\mathsf{A}}$, $\hat{\mathsf{S}}^{-1}\tilde{\mathsf{S}}$, and $\hat{\mathsf{X}}^{-1}\tilde{\mathsf{X}}$, where $\tilde{\mathsf{S}} = \mathsf{B}\hat{\mathsf{A}}^{-1}\mathsf{B}^\mathsf{T}$ and $\tilde{\mathsf{X}} = \mathsf{C}\hat{\mathsf{A}}^{-1}\mathsf{C}^\mathsf{T}$. We define

$$\gamma^A_{\min} = \lambda_{\min}(\hat{\mathsf{A}}^{-1}\bar{\mathsf{A}}), \qquad \gamma^A_{\max} = \lambda_{\max}(\hat{\mathsf{A}}^{-1}\bar{\mathsf{A}}), \qquad \gamma_A \in [\gamma^A_{\min}, \gamma^A_{\max}], \tag{74}$$

$$\gamma^S_{\min} = \lambda^+_{\min}(\hat{\mathsf{S}}^{-1}\tilde{\mathsf{S}}), \qquad \gamma^S_{\max} = \lambda_{\max}(\hat{\mathsf{S}}^{-1}\tilde{\mathsf{S}}), \qquad \gamma_S \in [\gamma^S_{\min}, \gamma^S_{\max}], \tag{75}$$

$$\gamma^X_{\min} = \lambda_{\min}(\hat{\mathsf{X}}^{-1}\tilde{\mathsf{X}}), \qquad \gamma^X_{\max} = \lambda_{\max}(\hat{\mathsf{X}}^{-1}\tilde{\mathsf{X}}), \qquad \gamma_X \in [\gamma^X_{\min}, \gamma^X_{\max}]. \tag{76}$$

We note that B is rank deficient by 1 and, consequently, the matrix $\tilde{\mathsf{S}}$ is symmetric positive semidefinite. Moreover, since $\hat{\mathsf{S}}^{-1}\tilde{\mathsf{S}}$ is similar to $\hat{\mathsf{S}}^{-\frac{1}{2}}\tilde{\mathsf{S}}\hat{\mathsf{S}}^{-\frac{1}{2}}$, which is a symmetric and positive semidefinite matrix, the eigenvalues of $\hat{\mathsf{S}}^{-1}\tilde{\mathsf{S}}$ are nonnegative and its smallest eigenvalue is equal to 0. However, since the presence of a zero eigenvalue does not affect the convergence of preconditioned GMRES, we focus only on the smallest positive eigenvalue, denoted as $\lambda^+_{\min}(\hat{\mathsf{S}}^{-1}\tilde{\mathsf{S}})$.
We then use the fact that looking for the eigenvalues of $\bar{\mathsf{P}}^{-1}\mathcal{A}_{\gamma\delta}$ is equivalent to solving

$$\bar{\mathsf{D}}^{-\frac{1}{2}}\mathcal{A}_{\gamma\delta}\bar{\mathsf{D}}^{-\frac{1}{2}}\mathsf{w} = \lambda\bar{\mathsf{D}}^{-\frac{1}{2}}\bar{\mathsf{P}}\bar{\mathsf{D}}^{-\frac{1}{2}}\mathsf{w}, \tag{77}$$

where

$$\bar{\mathsf{D}} := \begin{bmatrix} \hat{\mathsf{A}} & 0 & 0 \\ 0 & \hat{\mathsf{S}} & 0 \\ 0 & 0 & \hat{\mathsf{X}} \end{bmatrix}.$$

Let $\tilde{\mathsf{A}} := \hat{\mathsf{A}}^{-\frac{1}{2}}\bar{\mathsf{A}}\hat{\mathsf{A}}^{-\frac{1}{2}}$, $\mathsf{R} := \hat{\mathsf{S}}^{-\frac{1}{2}}\mathsf{B}\hat{\mathsf{A}}^{-\frac{1}{2}}$, and $\mathsf{K} := \hat{\mathsf{X}}^{-\frac{1}{2}}\mathsf{C}\hat{\mathsf{A}}^{-\frac{1}{2}}$. Since $\hat{\mathsf{A}}$, $\hat{\mathsf{S}}$, and $\hat{\mathsf{X}}$ are SPD, B is rank deficient by 1, and C has full row rank, then $\tilde{\mathsf{A}}$ is SPD, R has the same rank as B and K has full row rank. The explicit computation of (77) yields the following generalized eigenvalue problem:

$$\begin{bmatrix} \tilde{\mathsf{A}} & \mathsf{R}^\mathsf{T} & \mathsf{K}^\mathsf{T} \\ \mathsf{R} & 0 & 0 \\ \mathsf{K} & 0 & 0 \end{bmatrix} \begin{bmatrix} \mathsf{x} \\ \mathsf{y} \\ \mathsf{z} \end{bmatrix} = \lambda \begin{bmatrix} \mathsf{I} & \mathsf{R}^\mathsf{T} & \mathsf{K}^\mathsf{T} \\ 0 & -\mathsf{I} & 0 \\ 0 & 0 & -\mathsf{I} \end{bmatrix} \begin{bmatrix} \mathsf{x} \\ \mathsf{y} \\ \mathsf{z} \end{bmatrix}. \tag{78}$$

Let λ be an eigenvalue of $\bar{\mathsf{P}}^{-1}\mathcal{A}_{\gamma\delta}$ and $(\mathsf{x};\mathsf{y};\mathsf{z})$ a corresponding eigenvector such that $||\mathsf{x}||^2 + ||\mathsf{y}||^2 + ||\mathsf{z}||^2 = 1$. It follows from (78) that

$$\tilde{\mathsf{A}}\mathsf{x} - \lambda\mathsf{x} = (\lambda - 1)\mathsf{R}^\mathsf{T}\mathsf{y} + (\lambda - 1)\mathsf{K}^\mathsf{T}\mathsf{z}, \tag{79}$$

$$\mathsf{R}\mathsf{x} = -\lambda \mathsf{y}, \tag{80}$$

$$\mathsf{K}\mathsf{x} = -\lambda \mathsf{z}. \tag{81}$$

Following [28], we make the assumption that $1 \in [\gamma^A_{\min}, \gamma^A_{\max}]$, which is very commonly satisfied in practice. Since $\widehat{\mathsf{A}}^{-1}\bar{\mathsf{A}}$ is similar to $\tilde{\mathsf{A}}$, $\lambda = 1$ is also an eigenvalue of $\bar{\mathsf{P}}^{-1}\mathcal{A}_{\gamma\delta}$ with corresponding eigenvector $(\mathsf{x}; -\mathsf{R}\mathsf{x}; -\mathsf{K}\mathsf{x})$, provided that $\mathsf{x} \neq 0$. Hence, from now on we assume $\lambda \neq 1$ and $\mathsf{x} \neq 0$.

- $\mathsf{x} \in \ker(\mathsf{R}) \cap \ker(\mathsf{K})$.
  Eqs. (80) and (81) imply $\mathsf{y} = \mathsf{z} = 0$. Then, we readily obtain from (79)

  $$\tilde{\mathsf{A}}\mathsf{x} = \lambda \mathsf{x},$$

  which implies that λ is real and

  $$\lambda \in [\gamma^A_{\min}, \gamma^A_{\max}]. \tag{82}$$

  The associated eigenvector is of the form $(\mathsf{x}; 0; 0)$.

- $\mathsf{x} \in \ker(\mathsf{K}) \setminus \ker(\mathsf{R})$.
  Eq. (81) implies $\mathsf{z} = 0$, which gives

  $$\tilde{\mathsf{A}}\mathsf{x} - \lambda \mathsf{x} = (\lambda - 1)\mathsf{R}^{\mathsf{T}}\mathsf{y}, \tag{83}$$

  $$\mathsf{R}\mathsf{x} = -\lambda \mathsf{y}. \tag{84}$$

  After multiplying the first equation by x^*, the conjugate transpose of the second by y on the right, and inserting the second equation in the first we obtain

  $$\mathsf{x}^*\tilde{\mathsf{A}}\mathsf{x} - \lambda ||\mathsf{x}||^2 = -|\lambda|^2 ||\mathsf{y}||^2 + \bar{\lambda}||\mathsf{y}||^2.$$

  Using the fact that $||\mathsf{x}||^2 = 1 - ||\mathsf{y}||^2$, we get

  $$\mathsf{x}^*\tilde{\mathsf{A}}\mathsf{x} - \lambda + (\lambda - \bar{\lambda})||\mathsf{y}||^2 + |\lambda|^2||\mathsf{y}||^2 = 0. \tag{85}$$

  Writing now $\lambda = a + ib$, we obtain the following system for the real and imaginary parts

  $$\begin{cases} \mathsf{x}^*\tilde{\mathsf{A}}\mathsf{x} - a + (a^2 + b^2)||\mathsf{y}||^2 = 0, \\ b(2||\mathsf{y}||^2 - 1) = 0. \end{cases} \tag{86}$$

  From the second equation, it follows that $b = 0$, or $||\mathsf{y}||^2 = \frac{1}{2}$. We assume $b \neq 0$. Therefore, Eq. (85) in the system above reads as

  $$2\,\mathsf{x}^*\tilde{\mathsf{A}}\mathsf{x} - \lambda - \bar{\lambda} + |\lambda|^2 = 0 \tag{87}$$

  Exploiting the identity $|\lambda|^2 - \lambda - \bar{\lambda} = |\lambda - 1|^2 - 1$, and dividing the last equation by $\mathsf{x}^*\mathsf{x} = ||\mathsf{x}||^2 = \frac{1}{2}$, we get

  $$2|\lambda - 1|^2 = 2 - 2\frac{\mathsf{x}^*\tilde{\mathsf{A}}\mathsf{x}}{\mathsf{x}^*\mathsf{x}},$$

  therefore

  $$|\lambda - 1|^2 \leq 1 - \gamma^A_{\min}.$$

  Hence, if $1 - \gamma^A_{\min} \geq 0$, we have

  $$|\lambda - 1| \leq \sqrt{1 - \gamma^A_{\min}}. \tag{88}$$

  Conversely, if $1 - \gamma^A_{\min} < 0$, then there exists no λ with nonzero imaginary part satisfying equality (87). Using $\lambda = a + ib$, Eq. (88) can be written as

  $$(a - 1)^2 + b^2 \leq 1 - \gamma^A_{\min},$$

  which represents a circle centered in $(1, 0)$ with radius $\sqrt{1 - \gamma^A_{\min}}$, meaning that if $1 - \gamma^A_{\min} \geq 0$, then the eigenvalues λ lie in this circle.

  We now consider the case $b = 0$. In this case, λ is real, and the corresponding eigenvector can also be chosen to be real. Solving for x the Eq. (83) gives

  $$\mathsf{x} = \left(\tilde{\mathsf{A}} - \lambda \mathsf{I}\right)^{-1}(\lambda - 1)\mathsf{R}^{\mathsf{T}}\mathsf{y},$$

  which, plugged into Eq. (84) gives

  $$\mathsf{R}\left(\tilde{\mathsf{A}} - \lambda \mathsf{I}\right)^{-1}(1 - \lambda)\mathsf{R}^{\mathsf{T}}\mathsf{y} = \lambda \mathsf{y}. \tag{89}$$

  We now quote the following Lemma from [28], which will be used to characterized the real eigenvalues not lying in $[\gamma^A_{\min}, \gamma^A_{\max}]$.

Lemma 5.
Suppose that there exists an eigenvalue $\lambda \notin [\gamma^A_{min}, \gamma^A_{max}]$. Then, for arbitrary $z \neq 0$, there exists a vector $s \neq 0$ such that

$$\frac{z^T\left(\tilde{A} - \lambda I\right)^{-1} z}{z^T z} = \left(\frac{s^T \tilde{A} s}{s^T s} - \lambda\right)^{-1} = (\gamma_A - \lambda)^{-1} \tag{90}$$

where $\gamma_A := \frac{s^T \tilde{A} s}{s^T s}$.

Multiplying Eq. (89) by $\frac{y^T}{y^T y}$, we obtain

$$(1-\lambda)\,\frac{(R^T y)^T(\tilde{A} - \lambda I)^{-1}(R^T y)}{y^T y} = \lambda.$$

Using the lemma above, this yields

$$(1-\lambda)\,(\gamma_A - \lambda)^{-1}\,\frac{y^T R R^T y}{y^T y} = \lambda.$$

Note that, by the definition of R, we have $RR^T = \hat{S}^{-1/2}\tilde{S}\hat{S}^{-1/2}$, which is similar to $\hat{S}^{-1}\tilde{S}$. Therefore,

$$\frac{y^T R R^T y}{y^T y} \in [\gamma^S_{\min}, \gamma^S_{\max}],$$

and

$$(1-\lambda)(\gamma_A - \lambda)^{-1}\gamma_S = \lambda.$$

It follows that λ satisfies the quadratic equation

$$\lambda^2 - (\gamma_A + \gamma_S)\lambda + \gamma_S = 0.$$

The next steps are identical to the ones in [28], and are reported here only for completeness.

The two solutions of the quadratic equation above are

$$\lambda_{1,2} = \frac{\gamma_A + \gamma_S \pm \sqrt{(\gamma_A + \gamma_S)^2 - 4\gamma_S}}{2}.$$

The first root λ_1 can be bounded by

$$\lambda_1 = \frac{\gamma_A + \gamma_S + \sqrt{(\gamma_A + \gamma_S)^2 - 4\gamma_S}}{2} \leq \gamma_A + \gamma_S \leq \gamma^A_{\max} + \gamma^S_{\max},$$

while

$$\lambda_2 = \frac{2\gamma_S}{\gamma_A + \gamma_S + \sqrt{(\gamma_A + \gamma_S)^2 - 4\gamma_S}} \geq \frac{\gamma^S_{\min}}{\gamma^A_{\max} + \gamma^S_{\max}}.$$

All in all, we have

$$\lambda \in \left[\frac{\gamma^S_{\min}}{\gamma^A_{\max} + \gamma^S_{\max}}, \gamma^A_{\max} + \gamma^S_{\max}\right]. \tag{91}$$

- $x \in \ker(R) \setminus \ker(K)$.

Thanks to the particular form of the preconditioned system in (78), this case is completely analogous to the previous one. Therefore, we only report the final results.

Proceeding in the same fashion as in the previous paragraph, we have two cases to distinguish, depending on the solution b of Eq. (86). When $b \neq 0$: if $1 - \gamma^A_{\min} \geq 0$, we have

$$|\lambda - 1| \leq \sqrt{1 - \gamma^A_{\min}}. \tag{92}$$

If $b = 0$:

$$\lambda \in \left[\frac{\gamma^X_{\min}}{\gamma^A_{\max} + \gamma^X_{\max}}, \gamma^A_{\max} + \gamma^X_{\max}\right]. \tag{93}$$

- $x \notin \ker(R) \cup \ker(K)$.

We start by multiplying Eq. (79) by x^*, the conjugate transpose of Eq. (80) by y on the right, and the conjugate transpose of Eq. (81) by z on the right, obtaining

$$x^*\tilde{A}x - \lambda\|x\|^2 = (\lambda-1)x^*R^Ty + (\lambda-1)x^*K^Tz, \tag{94}$$

$$x^*R^Ty = -\bar{\lambda}\,\|y\|^2, \tag{95}$$

$$x^*K^Tz = -\bar{\lambda}\,\|z\|^2. \tag{96}$$

By insertion of the last two equations in (94) we get

$$x^*\tilde{A}x - \lambda||x||^2 = -(\lambda-1)\bar{\lambda}||y||^2 - (\lambda-1)\bar{\lambda}||z||^2,$$

which after simple algebra gives

$$x^*\tilde{A}x - \lambda||x||^2 = -|\lambda|^2(||y||^2 + ||z||^2) + \bar{\lambda}(||y||^2 + ||z||^2).$$

Using $||x||^2 + ||y||^2 + ||z||^2 = 1$ yields

$$x^*\tilde{A}x = \Big(|\lambda|^2 + \lambda - \bar{\lambda}\Big)||x||^2 + \bar{\lambda} - |\lambda|^2. \tag{97}$$

By writing $\lambda := a + ib$, we obtain the following equations for the real and imaginary parts:

$$\begin{cases} x^*\tilde{A}x - (a^2+b^2)||x||^2 - a + a^2 + b^2 = 0, \\ b(1 - 2||x||^2) = 0, \end{cases} \tag{98}$$

from which we get again $b = 0$, or $||x||^2 = \frac{1}{2}$. We assume $b \neq 0$, so that Eq. (97) becomes

$$2\,x^*\tilde{A}x = -|\lambda|^2 + \lambda + \bar{\lambda}. \tag{99}$$

Exploiting again the identity $|\lambda|^2 - \lambda - \bar{\lambda} = |\lambda - 1|^2 - 1$, and dividing the last equation by $x^*x = ||x||^2 = \frac{1}{2}$, we get

$$|\lambda - 1|^2 = 1 - \frac{x^*\tilde{A}x}{x^*x},$$

therefore

$$|\lambda - 1|^2 \leq 1 - \gamma^A_{\min}.$$

Hence, if $1 - \gamma^A_{\min} \geq 0$, we have

$$|\lambda - 1| \leq \sqrt{1 - \gamma^A_{\min}}. \tag{100}$$

If $1 - \gamma^A_{\min} < 0$, then there exists no λ with nonzero imaginary part satisfying (99).

We finally consider the case $b = 0$. From Eqs. (80) and (81) we immediately obtain

$$y = -\frac{1}{\lambda}Rx, \qquad z = -\frac{1}{\lambda}Kx.$$

Plugging these into Eq. (79), we get

$$\tilde{A}x - \lambda x = -\frac{(\lambda-1)}{\lambda}R^TRx - \frac{(\lambda-1)}{\lambda}K^TKx,$$

then we multiply both sides by $\frac{\lambda x^T}{x^Tx}$, obtaining the following quadratic equation in λ:

$$\lambda^2 - \lambda\Big(\frac{x^T\tilde{A}x}{x^Tx} + \frac{x^TR^TRx}{x^Tx} + \frac{x^TK^TKx}{x^Tx}\Big) + \Big(\frac{x^TR^TRx}{x^Tx} + \frac{x^TK^TKx}{x^Tx}\Big) = 0. \tag{101}$$

We now define

$$\gamma_R := \frac{x^TR^TRx}{x^Tx} \quad \text{and} \quad \gamma_K := \frac{x^TK^TKx}{x^Tx}.$$

Therefore,

$$\lambda^2 - \lambda(\gamma_A + \gamma_R + \gamma_K) + \gamma_R + \gamma_K = 0. \tag{102}$$

Solving for λ gives the following two (real) solutions:

$$\lambda_{1,2} = \frac{\gamma_A + \gamma_R + \gamma_K \pm \sqrt{(\gamma_A + \gamma_R + \gamma_K)^2 - 4(\gamma_R + \gamma_K)}}{2}.$$

The first root λ_1 can be bounded by

$$\lambda_1 = \frac{\gamma_A + \gamma_R + \gamma_K + \sqrt{(\gamma_A + \gamma_R + \gamma_K)^2 - 4(\gamma_R + \gamma_K)}}{2} \leq \gamma_A + \gamma_R + \gamma_K \leq \gamma^A_{\max} + \gamma^R_{\max} + \gamma^K_{\max},$$

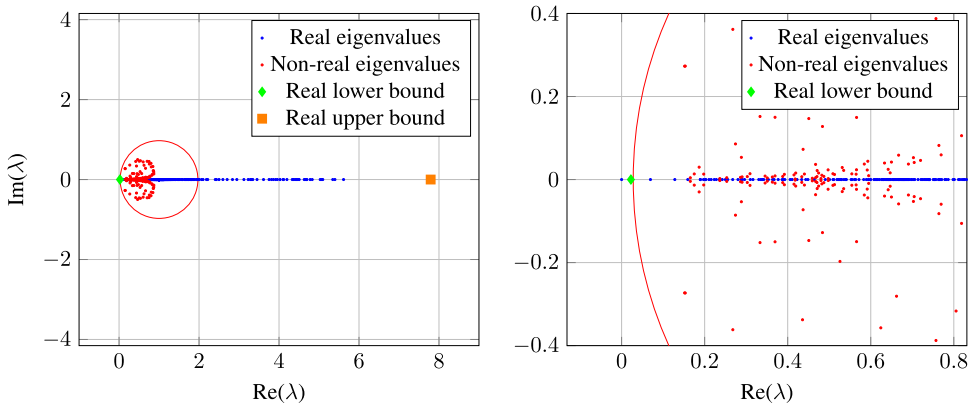

(a) Whole spectrum of preconditioned matrix. (b) Zoom on the leftmost part of the spectrum.

Fig. 5. Numerical check of the bounds for the preconditioned matrix when an inexact variant of the preconditioner is employed.

while

$$\lambda_2 = \frac{2(\gamma_R + \gamma_K)}{(\gamma_A + \gamma_R + \gamma_K) + \sqrt{(\gamma_A + \gamma_R + \gamma_K)^2 - 4(\gamma_R + \gamma_K)}} \geq \frac{\gamma^R_{\min} + \gamma^K_{\min}}{\gamma^A_{\max} + \gamma^R_{\max} + \gamma^K_{\max}}.$$

From the singular value decomposition of R it follows that the nonzero eigenvalues of $\mathsf{R}^\mathsf{T}\mathsf{R}$ and $\mathsf{K}^\mathsf{T}\mathsf{K}$ are the same ones of $\mathsf{R}\mathsf{R}^\mathsf{T}$ and $\mathsf{K}\mathsf{K}^\mathsf{T}$, respectively. Therefore, we have

$$\gamma_R \in [0, \gamma^S_{\max}] \quad \text{and} \quad \gamma_K \in [0, \gamma^X_{\max}].$$

Moreover, the assumption $\mathsf{x} \notin \ker(\mathsf{R}) \cup \ker(\mathsf{K})$ means that we are effectively working in the space where $\mathsf{R}^\mathsf{T}\mathsf{R}$ and $\mathsf{K}^\mathsf{T}\mathsf{K}$ are strictly positive definite, thus $\gamma_R > 0$ and $\gamma_K > 0$. More precisely, we have $\gamma_R \in [\gamma^S_{\min}, \gamma^S_{\max}]$. The very same argument applies to γ_K, allowing to write

$$\lambda_2 \geq \frac{\gamma^S_{\min} + \gamma^X_{\min}}{\gamma^A_{\max} + \gamma^S_{\max} + \gamma^X_{\max}} > 0.$$

We conclude that

$$\lambda \in \left[\frac{\gamma^S_{\min} + \gamma^X_{\min}}{\gamma^A_{\max} + \gamma^S_{\max} + \gamma^X_{\max}}, \gamma^A_{\max} + \gamma^S_{\max} + \gamma^X_{\max} \right]. \tag{103}$$

5.1. Spectrum of the matrix preconditioned with the inexact variant of $\mathcal{P}_{\gamma\delta}$

We verify the correctness of the bounds using the same configuration as in Section 4.1. As an inexact variant of the *ideal* preconditioner in (32), we consider the case in which we approximate the mass matrices on the pressure and multiplier space with diagonal matrices. In particular, we consider $\widehat{\mathsf{M}}_\mathsf{p} := \mathrm{diag}(\mathsf{M}_\mathsf{p})$, which is a widely used choice in the context of the classical Stokes problem [18], and $\widehat{\mathsf{M}}_\lambda := \mathrm{diag}(\mathsf{M}_\lambda)^2$. As an approximation for $\mathsf{A}_{\gamma\delta}$, we employ its incomplete Cholesky factorization, computed using the `ichol` function in MATLAB with a drop tolerance set to 10^{-1}. Note that for the numerical experiments reported in Section 6, the augmented (1,1)-block is always inverted using a CG solver preconditioned by a single V-cycle of AMG, with a loose tolerance of 10^{-2}, whereas the inversion of M_p is performed using a CG solver preconditioned by the lumped pressure mass matrix. However, to verify the theoretical findings, here different approximations are considered for the augmented block $\mathsf{A}_{\gamma\delta}$ and for M_p, for simplicity of implementation.

To summarize, the following (positive definite) approximations for $\bar{\mathsf{A}}$, S, and X are considered:

- $\widehat{\mathsf{A}} := \mathrm{ichol}(\bar{\mathsf{A}}, \mathrm{drop\_tol} = 10^{-1})$,
- $\widehat{\mathsf{S}} := \frac{1}{\gamma}\mathrm{diag}(\mathsf{M}_\mathsf{p})$,
- $\widehat{\mathsf{X}} := \frac{1}{\delta}\mathrm{diag}(\mathsf{M}_\lambda)^2$.

We show in Fig. 5 the spectrum of the preconditioned matrix $\bar{\mathsf{P}}^{-1}\mathcal{A}_{\gamma\delta}$ when the inexact variant above is employed. In particular, we show the lower (green diamond) and upper (orange square) bound for the real eigenvalues. We notice how the lower and upper bounds for the real part of the spectrum confirm the theoretical findings above. As already explained, $\lambda = 0$ is an eigenvalue of the original system, and hence it coincides with the numerical lower bound. Moreover, it is evident how all the imaginary eigenvalues are well-contained in the disk of radius $\sqrt{1 - \gamma^{\mathsf{A}}_{\min}}$.

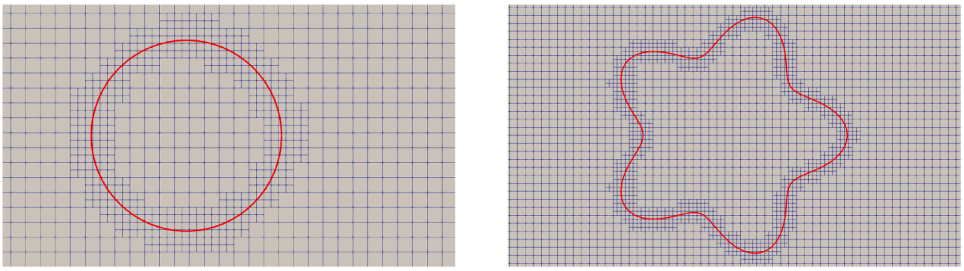

(a) (b)

Fig. 6. Zoom on pre-processed background grid Ω_h for the circle interface $\Gamma = \Gamma^1$ (left) and the flower-shaped interface $\Gamma = \Gamma^2$ (right).

6. Numerical experiments

In this Section, we present a series of numerical experiments to assess the performance of the proposed AL-based preconditioners for the problems analyzed in this work. All the experiments have been performed using the C++ finite element library DEAL.II [42,43] and are available at a maintained GitHub repository provided by the authors[2]. Building on top of a generic library, we can exploit (in a dimension-independent fashion) features such as adaptive mesh refinement, higher-order elements, handling of non-matching meshes, hanging node constraints, as well as API to high-performance preconditioners provided by state-of-the-art linear algebra libraries such as TRILINOS [54] and PETSc [55]. Our code is memory-distributed and builds on the Message Passing Interface (MPI) communication model [56].

In the examples involving the Poisson problem, we employ $\mathcal{Q}_1$ elements both for the background space V_h and the immersed space Λ_h. For the Stokes test case, we employ the classical Taylor-Hood $\mathcal{Q}_2$-$\mathcal{Q}_1$ stable pair for the velocity and pressure spaces V_h and Q_h, and $\mathcal{Q}_1$ elements for the multiplier space Λ_h. In the forthcoming Tables, we will denote by $|V_h| + |\Lambda_h|$ the total number of DoF, which corresponds to the global size of the linear system in (11). Similarly, for the Stokes problem, we denote with $|V_h| + |Q_h| + |\Lambda_h|$ the total number of DoF associated with the linear system in (31). All tests are performed using background meshes made of quadrilaterals or hexahedra and immersed boundary meshes made of segments and quadrilaterals. We perform an initial pre-processing of the background grid Ω_h by applying a localized refinement around the interface, where most of the error is concentrated [7]. Sample two-dimensional grids resulting from this process in the two-dimensional case are shown in Fig. 6. A three-dimensional analogue is displayed in Fig. 14a. As we are using conforming elements on quadrilateral or hexahedral meshes for the background domain, local refinement procedures induce the presence of hanging nodes. As usual, the discrete solution is enforced to be continuous through constraints on the nodal coefficients. In practice, the nodal unknowns associated with those nodes are eliminated by restricting their value to an interpolation of the nodal values of the finite element unknown in its parent element. The interested reader is referred to [42] for the implementation details. Finally, we investigate the iteration counts under simultaneous refinement of both the background and immersed meshes. All the solvers are started with the zero vector as initial guess. Throughout the experiments, we will set $\mathsf{Q} = \mathsf{M}_\mathsf{p}$, $\mathsf{W} = \mathsf{M}^2_\lambda$, and we will consider absolute tolerances TOL ranging from 10^{-8} to 10^{-10}.

6.1. Poisson problem

We analyze different preconditioning techniques for the linear system (8). In particular, we test three approaches which can be applied to our context: BFBt preconditioning [57], rational preconditioning [23], and the AL-based preconditioner devised in Section 2.2.

Unless stated otherwise, the resulting linear system (8) (or the equivalent augmented version (11)) is solved with FGMRES(30), preconditioned by each one of the preconditioners defined above. For ease of presentation, we recall here the definition of the first two preconditioners. With the BFBt approach, the action of the preconditioner is defined as

$$\mathcal{P}^{-1}_{\text{BFBt}} = \begin{bmatrix} \widehat{\mathsf{A}} & \mathsf{C}^\mathsf{T} \\ 0 & -\widehat{\mathsf{S}} \end{bmatrix}^{-1},$$

where $\widehat{\mathsf{S}}^{-1} := (\mathsf{C}\mathsf{C}^\mathsf{T})^{-1}\mathsf{C}\mathsf{A}\mathsf{C}^\mathsf{T}(\mathsf{C}\mathsf{C}^\mathsf{T})^{-1}$. Similar to what was reported in [57], the following set of experiments shows that convergence rates for the BFBt preconditioner are mesh-dependent, with iteration counts increasing in proportion to $h_\Omega^{-\frac{1}{2}}$. The action of $\widehat{\mathsf{A}}^{-1}$ is computed through a conjugate gradient solver, preconditioned by AMG, with inner tolerance set to 10^{-2}.

When employing the rational-based preconditioner [22,23], its action on a vector is determined by the following inverse

$$\mathcal{P}^{-1}_{\text{rational}} := \begin{bmatrix} \widehat{\mathsf{A}} & 0 \\ 0 & \widehat{\mathsf{S}} \end{bmatrix}^{-1}.$$

[2] Available at https://github.com/fdrmrc/fictitious_domain_AL_preconditioners.

This approach is based on the observation that the Schur complement $\mathsf{S} = \mathsf{C}\mathsf{A}^{-1}\mathsf{C}^{\mathsf{T}}$, in the context of matching interfaces, is spectrally equivalent to the fractional Laplacian [22]. The action of the inverse of $\widehat{\mathsf{S}}$ on a vector v is computed using a rational approximation and reads

$$\widehat{\mathsf{S}}^{-1}\mathsf{v} = c_0\mathsf{M}_\lambda^{-1}\mathsf{v} + \sum_{i=1}^{N_p} c_i\left(\mathsf{A}_\lambda - \rho p_i \mathsf{M}_\lambda\right)^{-1}\mathsf{v},$$

where c_i and p_i are residues and poles, respectively, A_λ is the stiffness matrix on the immersed space Λ_h, and ρ denotes the spectral radius of $\mathsf{M}_\lambda^{-1}\mathsf{A}_\lambda$. From the implementation standpoint, $\{p_i\}_{i=1}^{N_p}$ and $\{c_i\}_{i=0}^{N_p}$ are computed offline once and for all. In the present case, $N_p = 20$. We also need an upper bound on $\rho(\mathsf{M}_\lambda^{-1}\mathsf{A}_\lambda)$, which we estimate as in [23] with

$$\rho(\mathsf{M}_\lambda^{-1}\mathsf{A}_\lambda) \le d(d+1)||\mathrm{diag}(\mathsf{M}_\lambda)^{-1}||_\infty ||\mathsf{A}||_\infty.$$

Moreover, as $p_i \in \mathbb{R}$, $p_i \le 0$, the application of $\widehat{\mathsf{S}}^{-1}$ involves a series of N_p elliptic problems for which AMG is well-suited. The solution of every shifted linear system is realized using the CG method with AMG as a preconditioner and a strict tolerance of 10^{-14}. We observed that employing FGMRES as outer solver, with looser inner tolerances for these sub-systems, leads to high iteration counts in this case. The inversion of $\widehat{\mathsf{A}}^{-1}$ in the $(1,1)$-block is done through the sparse direct solver UMFPACK. Since the preconditioner is SPD, the outer solver associated with the rational preconditioner is chosen to be MINRES [58].
Concerning the AL preconditioner, we set $\gamma = 10$ and a low inner tolerance of 10^{-2} for the augmented block $\widehat{\mathsf{A}}_\gamma$ which is always inverted through a CG solver preconditioned by a single V-cycle of AMG. The inversion of W is performed through the sparse direct solver UMFPACK. Moreover, the absolute tolerance employed in these experiments is $\mathrm{TOL} = 10^{-10}$. We notice that we have chosen a rather strict tolerance compared to other papers analyzing preconditioners, which leads to higher iteration numbers. We have chosen this convergence criterion because it makes seeing trends easier due to the higher number of outer iterations. When using AMG, we adopt the TrilinosML implementation [54], with parameters shown in Table C.1, in Appendix C.

We fix $\Omega = [0,1]^2$ as the background domain and consider various immersed domains $\{\Gamma^i\}_{i=1,2,3}$ of different shapes originating from an unfitted discretization of different curves:

- $\Gamma^1 := \partial B_r(\boldsymbol{c})$,
- $\Gamma^2 := \left\{ \left(R + x_c + r\cos(\theta\pi x)\cos(2\pi x),\ R + y_c + r\cos(\theta\pi x)\sin(2\pi x)\right) \,\middle|\, x \in [0,1) \right\}$,
- $\Gamma^3 := \left\{(x,y) \in \mathbb{R}^2 : \min(x-a, b-x, y-a, b-y) = 0 \mid (x,y) \in [0,1]^2\right\}$,

where the second curve is a parametrization of a flower-like interface and the last one is the boundary of the square $[a,b]^2$, assuming $a > 0$ and $a < b < 1$. In all the numerical results reported hereafter, we set $f = 1$ and $g = 1$ as data. Note that we have also tested various other data and observed the same trends and behavior for the three preconditioners considered. We point out that, in all experiments, the number of outer MINRES iterations needed by the rational preconditioner with lower tolerances (such as $\mathrm{TOL} = 10^{-6}$) is significantly lower and agrees with the findings already reported in [22,23]. The correctness of our implementation can be verified in Table 1 and Fig. 7, where optimal convergence rates against the mesh size h_Ω are reported for the manufactured solution $u(x,y) := \sin(2\pi x)\sin(2\pi y)$, which in turn implies $f := 8\pi u^2(x,y)$. Notice that from the smoothness of u, it follows that in this case the Lagrange multiplier is identically zero. This corresponds to a special case where the interface is not truly an interface. Indeed, when an

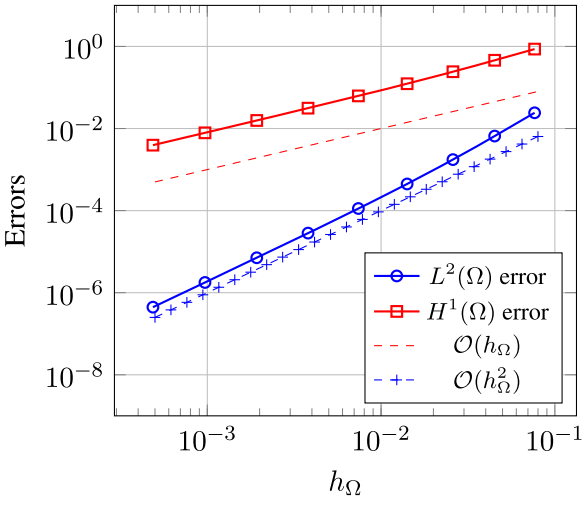

Fig. 7. $L^2(\Omega)$ and $H^1(\Omega)$ errors against h_Ω for interface Γ^1.

Table 1
$L^2(\Omega)$ and $H^1(\Omega)$ errors for Γ^1 across mesh refinement for the manufactured solution $u(x,y) := \sin(2\pi x)\sin(2\pi y)$.

Convergence history for Γ^1

DoF $(\lvert V_h\rvert + \lvert\Lambda_h\rvert)$	$L^2(\Omega)$ rate	$H^1(\Omega)$ rate
171 + 17	2,4158e-02	8,6193e-01
493 + 33	6,5512e-03	4,5953e-01
1,489 + 65	1,7482e-03	2,4187e-01
5,013 + 129	4,4547e-04	1,2336e-01
18,237 + 257	1,1254e-04	6,2321e-02
69,259 + 513	2,8308e-05	3,1324e-02
269,563 + 1,025	7,0960e-06	1,5702e-02
1,063,467 + 2,049	1,7755e-06	7,8602e-03
4,223,931 + 4,097	4,4425e-07	3,9325e-03

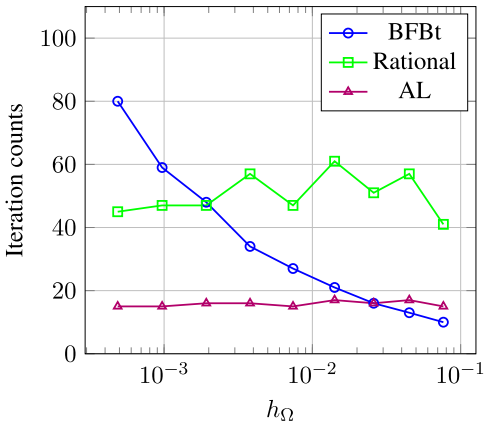

Fig. 8. Iteration counts vs. h_Ω for Γ^1.

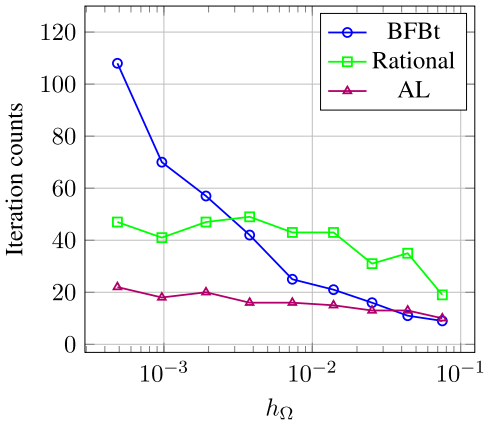

Fig. 9. Iteration counts vs. h_Ω for Γ^2.

Table 2
Outer iteration counts for the Poisson problem with circular interface Γ^1.

Outer iteration counts for Γ^1

DoF $(\lvert V_h\rvert + \lvert\Lambda_h\rvert)$	BFBt	Rational	AL
171 + 17	10	41	15
493 + 33	13	57	17
1,489 + 65	16	51	16
5,013 + 129	21	61	17
18,237 + 257	27	47	15
69,259 + 513	34	57	16
269,563 + 1,025	48	47	16
1,063,467 + 2,049	59	47	15
4,223,931 + 4,097	80	45	15

Table 3
Outer iteration counts for the Poisson problem with flower-shaped interface Γ^2.

Outer iteration counts for Γ^2

DoF $(\lvert V_h\rvert + \lvert\Lambda_h\rvert)$	BFBt	Rational	AL
177 + 17	9	19	10
518 + 33	11	35	13
1,567 + 65	16	31	13
5,177 + 129	21	43	15
18,575 + 257	25	43	16
69,869 + 513	42	49	16
270,845 + 1,025	57	47	20
1,065,947 + 2,049	70	41	18
4,229,139 + 4,097	108	47	22

arbitrary value for u is imposed on Γ, it cannot be expected that the solution is in $H^2(\Omega)$ since its gradient is not a continuous function across the interface. In such cases, it is known that non-matching methods are not able to recover the optimal rate of convergence [7]. The chosen value for the absolute tolerance TOL is comparable, if not stricter, to the possible accuracy obtained in the smooth case by the method.

Tables 2–4 present the outer iteration counts upon mesh-refinement for the Poisson problem (8) using the three preconditioners outlined above. As interfaces we consider the circular interface Γ^1, centered at $c = (0.4, 0.4)$ with radius $r = 0.2$, the flower-shaped interface Γ^2, where we have chosen $R = 0.2$, $r = 0.04$, $x_c = 0.5$, $y_c = 0.5$, $\theta = 10$, and the square interface Γ^3 defined by parameters $a = 0.25$ and $b = 0.5$. The results demonstrate that the AL preconditioner consistently requires fewer outer iterations compared to BFBt and rational approaches, highlighting its robustness and efficiency. As the number of DoF increases, the iteration counts for the BFBt preconditioner show a noticeable increase, confirming the dependency on the mesh size. In contrast, the rational and AL preconditioners exhibit robust iteration counts, with the AL preconditioner showing lower numbers. This can be better appreciated in Figs. 8–10, where the iteration counts are plotted against the mesh size of the background h_Ω. For what concerns the inner solves for $\widehat{\mathrm{A}}_\gamma$ we observed a roughly constant and low number of iteration counts across every refinement cycle, never exceeding nine CG iterations for each outer iteration of FGMRES(30). The low number of outer iterations required by the AL-based preconditioner (combined with the low number of inner ones) yields overall good solution times. For the sequence of refinements performed in Table 2, we measured the wall-clock time spent in the solver[3] by all the preconditioners presented in this Section. The times are reported in Fig. 11. Compared with BFBt and the rational preconditioner, the AL-based approach exhibits lower times across all

[3] On a 2.60GHz Intel Xeon processor, using a Release build with optimization flags enabled.

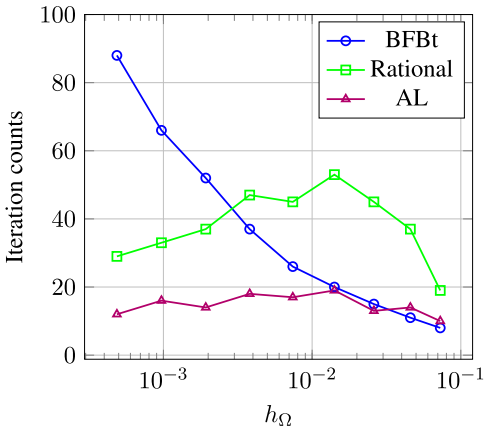

Fig. 10. Iteration counts vs. h_Ω for Γ^3.

Table 4
Outer iteration counts for the Poisson problem with square interface Γ^3.

Outer iteration counts for Γ^3			
DoF $(\lvert V_h\rvert + \lvert\Lambda_h\rvert)$	BFBt	Rational	AL
189 + 17	8	19	10
477 + 33	11	37	14
1,477 + 65	15	45	13
5,013 + 129	20	53	19
18,189 + 257	26	45	17
69,117 + 513	37	47	18
269,317 + 1,025	52	37	14
1,062,933 + 2,049	66	33	16
4,222,989 + 4,097	88	29	12

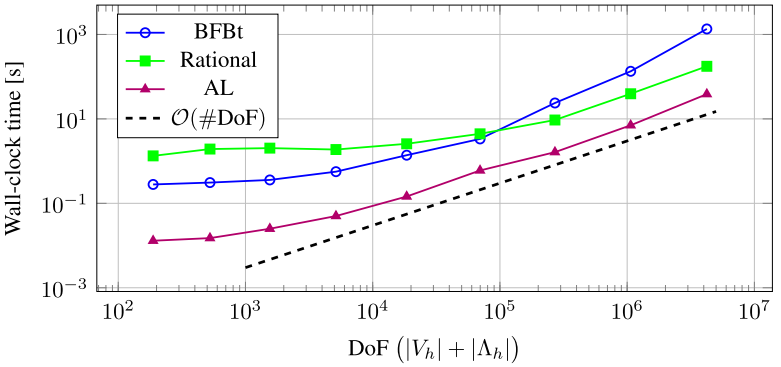

Fig. 11. Wall-clock time (in seconds) for the Poisson problem with circular interface Γ^1 using different preconditioners, as a function of the total number of DoF.

the refinement cycles. Similar trends were observed for all other interfaces, so additional figures and tables are omitted. Albeit a systematic comparison of the solvers is out of the scope of this paper, we argue that the observed times are representative.

6.2. Stokes problem

We analyze the application to the Stokes problem of the AL preconditioner $\mathcal{P}_{\gamma\delta}$ developed in Section 3. The background domain is fixed to be $\Omega = [0,1]^2$, and the following configuration is considered:

$$\mathbf{f} := [1,0]^T, \quad \mathbf{g} := [-0.5, 0.5]^T, \quad \Gamma^4 := \partial B_r(\boldsymbol{c}),$$

where $\boldsymbol{c} = (0.45, 0.45)$ and $r = 0.21$. Notice that $\mathbf{g}$ has been chosen in such a way that the compatibility condition (19) is automatically satisfied. Concerning the AL parameters, we have set $\gamma = \delta = 10$. In this two-dimensional example, the inversion of the mass matrices Q and W is performed through the sparse direct solver UMFPACK, as we are still in a regime for which the factorization of the pressure mass matrix Q is affordable. Notice that W is a 1D mass matrix, so its explicit inversion with a sparse direct solver does not constitute a possible bottleneck in this example, even when the cardinality of V_h is large. The augmented term is never factorized, but is always inverted through a CG solver preconditioned by a single V-cycle of AMG, with a loose tolerance of 10^{-2}. The iteration counts for the outer FGMRES(30) solver are reported in Table 5a, corresponding to an absolute tolerance of $\text{TOL} = 10^{-8}$. The AL preconditioner shows a robust behavior, requiring low FGMRES(30) iteration counts which are independent of the refinement levels. We display the inner iterations as the average over all outer FGMRES(30) iterations of the number of iterations for the augmented velocity block $\widehat{\mathsf{A}}_\gamma$. From there it can be seen that the number of inner iterations slightly increases upon mesh refinement, but remains essentially bounded. The development of a γ, δ-robust and mesh-independent solver for our double-augmented block $\widehat{\mathsf{A}}_{\gamma\delta}$ is far from trivial and is left for future work. Ad-hoc geometric multigrid schemes have been used and developed in [39,59] in the context of Oseen and Stokes problems, respectively, to overcome the issues introduced by the augmentation.

Table 5
Outer FGMRES(30) iteration counts with an absolute tolerance TOL = 10^{-8}, along with the corresponding number of average inner iterations for the Stokes problem using AL preconditioner across different geometries and solvers.

Iteration counts for Γ^4 (direct solvers)		
DoF $(\lvert V_h\rvert + \lvert Q_h\rvert + \lvert \Lambda_h\rvert)$	Outer	Inner
518 + 72 + 18	17	7
1,446 + 190 + 34	16	8
3,818 + 494 + 66	16	16
11,922 + 1,523 + 130	16	18
40,002 + 5,065 + 258	15	21
145,442 + 18,309 + 514	15	24
2,154,546 + 269,831 + 2,050	10	31
8,503,490 + 1,063,961 + 4,098	10	42

(a) Circular interface Γ^4 (2D test).

Iteration counts for Γ^4 (inexact solvers)		
DoF $(\lvert V_h\rvert + \lvert Q_h\rvert + \lvert \Lambda_h\rvert)$	Outer	Inner
518 + 72 + 18	18	2
1,446 + 190 + 34	20	2
3,818 + 494 + 66	20	13
11,922 + 1,523 + 130	21	15
40,002 + 5,065 + 258	20	18
145,442 + 18,309 + 514	19	20
2,154,546 + 269,831 + 2,050	12	25
8,503,490 + 1,063,961 + 4,098	11	28

(b) Circular interface Γ^4 (2D test).

Iteration counts for Γ^5		
DoF $(\lvert V_h\rvert + \lvert Q_h\rvert + \lvert \Lambda_h\rvert)$	Outer	Inner
9,435+469+24	12	13
22,131+1,073+192	12	16
135,951+6,171+294	12	24
904,143+39,475+3,072	12	24
6,718,791+286,855+4,614	8	37
52,077,519+2,197,115+286,855	8	50

(c) Spherical interface Γ^5 (3D test).

Iteration counts for Γ^6		
DoF $(\lvert V_h\rvert + \lvert Q_h\rvert + \lvert \Lambda_h\rvert)$	Outer	Inner
8,367+421+48	13	10
32,829+1,561+192	14	11
149,319+6,767+768	14	17
984,387+42,961+3,072	14	19
7,132,467+304,897+12,288	13	25
53,641,515+2,265,401+49,152	13	28

(d) Toroidal interface Γ^6 (3D test).

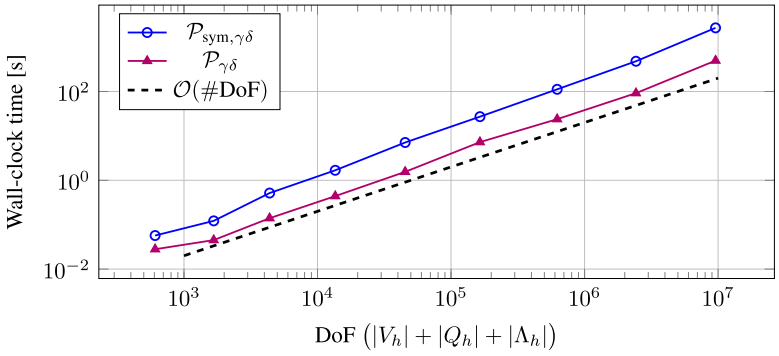

Fig. 12. Wall-clock time (in seconds) for the Stokes problem with circular interface Γ^4 using the block-triangular AL preconditioner $\mathcal{P}_{\gamma\delta}$ and its SPD variant $\mathcal{P}_{\text{sym},\gamma\delta}$, as a function of the total number of DoF.

Having confirmed the good behavior of the preconditioner with direct solvers, we test its performance when the action of Q^{-1} and W^{-1} is applied inexactly. The inversion of Q is performed with a CG solver preconditioned by the (lumped) pressure mass matrix $\widehat{\mathsf{M}}_\mathsf{p}$, while for the matrix W we directly invert its diagonal approximation (see Eq. (17)) . We show in Table 5b the results with this approach. The usage of iterative solvers also for the mass matrices does not spoil the overall quality of the preconditioner. We observe only a marginal increase in the number of outer iterations compared to the case where exact inversions are performed. However, the overall numbers are robust upon mesh refinement, with a considerable saving in computational cost associated with the fact that no direct inversion of any block has been performed. The computed velocity field $\mathbf{u}$ and its streamlines are shown in Fig. 13. Finally, we test the performance of the block triangular preconditioner $\mathcal{P}_{\gamma\delta}$ defined in (32) against the diagonal and SPD variant $\mathcal{P}_{\text{sym},\gamma\delta}$ presented in Remark 4, which is used as a preconditioner for MINRES. The computing times for the solver are reported in Fig. 12, where it can be appreciated how the block triangular preconditioner $\mathcal{P}_{\gamma\delta}$ outperforms the diagonal variant by approximately an order of magnitude.

6.2.1. *Three-dimensional tests*

In order to show the reliability of our preconditioner also for practical usage, we finally consider the three-dimensional extension of the tests in the previous paragraph. The following embedded surfaces are tested:

- $\Gamma^5 := \partial B_r(\boldsymbol{c})$,

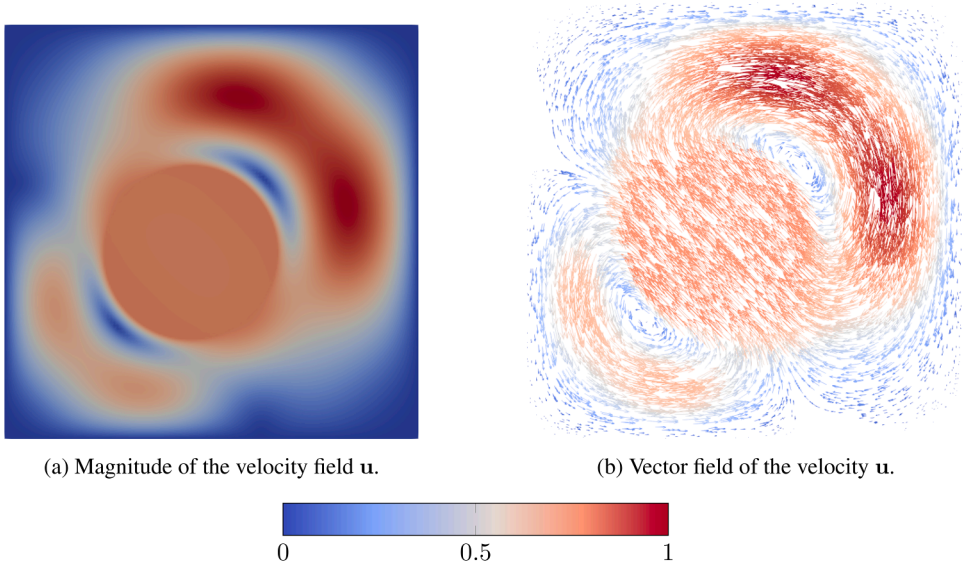

(a) Magnitude of the velocity field $\mathbf{u}$. (b) Vector field of the velocity $\mathbf{u}$.

Fig. 13. Computed vector field $\mathbf{u}$ for the Stokes problem with an embedded circular interface.

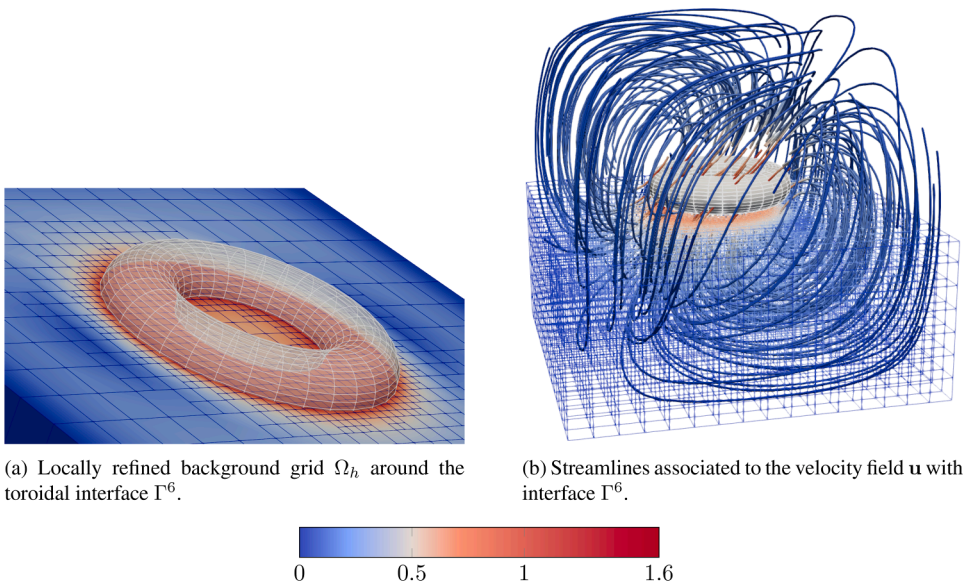

(a) Locally refined background grid Ω_h around the toroidal interface Γ^6. (b) Streamlines associated to the velocity field $\mathbf{u}$ with interface Γ^6.

Fig. 14. Post-processing of the velocity field $\mathbf{u}$ with interface Γ^6. On the right, the background geometry is shown with a wireframe (and clipped) representation.

- $\Gamma^6 := \left\{(x,y,z) \in \mathbb{R}^3 : \left(\sqrt{x^2+y^2} - 0.3\right)^2 + z^2 - (0.1)^2 = 0\right\}$,

where $\boldsymbol{c} = (\frac{1}{2}, \frac{1}{2}, \frac{1}{2})$ and $r = 0.1$. The interface Γ^6 describes a torus with inner and outer radius of 0.2 and 0.4. As data of the problem, we consider

$$\mathbf{f} := [1,0,0]^T, \quad \mathbf{g} := [-1,1,0]^T.$$

A sample grid illustrating the (local) refinement process near the embedded toroidal surface mesh Γ^6 is shown in Fig. 14a, while Fig. 14b displays the streamlines for the computed velocity field $\mathbf{u}$. The AL parameters are set to $\gamma = \delta = 10$. The $(1,1)$-block is solved as in the previous tests with a tolerance of 10^{-2}. The mass matrices Q and W are inverted iteratively in the same way as explained in the previous two-dimensional test. The results of this study are reported in Table 5c and d. For both the interfaces, we observe outer iteration counts independent of the refinement level. Moreover, the order of magnitude of the inner AMG iterations for the inversion of the $(1,1)$-block is the same as in the two-dimensional tests. We solve problems up to 56 million of unknowns, thereby confirming the trends observed so far. The three-dimensional simulations have been run varying the number of MPI processes employed from

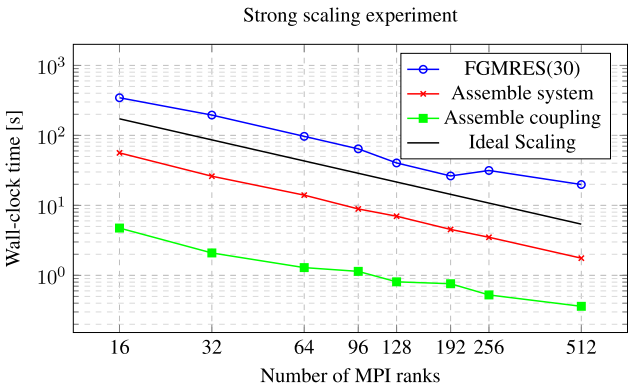

Fig. 15. Strong scaling test of the principal components of the whole solver for a three-dimensional problem with interface Γ^6 with 7 million DoF.

16 up to 256 and observing robust inner and outer iteration counts. Notably, the largest simulations in Table 5c and d must be run with a sufficiently large number of cores due to the high memory cost associated with the setup of the AMG preconditioner for the augmented block and the storage of sparse matrices arising from higher-order discretizations. We show in Fig. 15 a strong scaling experiment for different components of our pipeline, where we keep a fixed problem size resulting from a three-dimensional discretization comprising roughly 7 million DoF and increase incrementally the number of MPI processes from 16 to 512. In particular, we measure the wall-clock time to assemble matrices A and B for the Stokes problem, the time to assemble the coupling matrix C, and the time taken by FGMRES(30) to solve the final linear system of equations. The parallel experiments have been performed on the Galileo100[4] Italian supercomputer. Its compute nodes have two sockets (each one with 24 cores of Intel CascadeLake). Good scaling properties are confirmed for all the kernels employed in the simulation.

7. Conclusions

We have presented augmented Lagrangian-based preconditioners to accelerate the convergence of iterative solvers for linear systems arising from the finite element method applied to the fictitious domain approach. We have considered two model problems with an internal interface, namely the Poisson problem and the Stokes problem, which yield two-by-two and three-by-three block systems, respectively. A spectral analysis of the preconditioner for the Stokes problem has been performed in both the exact and the inexact case. We tested practical and cheap variants of the proposed preconditioner that do not require the usage of sparse direct solvers, showing its effectiveness through several numerical tests in two and three dimensions and with different immersed geometries. Additionally, the memory-distributed implementation was validated in a three-dimensional context. Future work will focus on extending such techniques to more complex systems arising from fictitious domain methodologies, such as elliptic interface problems, which are currently under investigation, and the development of tailored solution strategies for the inversion of the augmented block.

CRediT authorship contribution statement

Michele Benzi: Writing – review & editing, Supervision, Methodology, Funding acquisition, Conceptualization; **Marco Feder:** Writing – review & editing, Writing – original draft, Validation, Software, Methodology, Formal analysis, Conceptualization; **Luca Heltai:** Writing – review & editing, Supervision, Methodology, Funding acquisition, Conceptualization; **Federica Mugnaioni:** Writing – review & editing, Writing – original draft, Validation, Software, Methodology, Formal analysis, Conceptualization.

Data availability

The code is available on GitHub and is referenced within the manuscript.

Declaration of competing interest

The authors declare that they have no known competing financial interests or personal relationships that could have appeared to influence the work reported in this paper.

Acknowledgments

MB acknowledges partial support from grant MUR PRIN 2022 No. 20227PCCKZ (“Low Rank Structures and Numerical Methods in Matrix and Tensor Computations and their Applications“). LH and MF acknowledge partial support from grant MUR PRIN 2022

[4] For the technical specifications, see https://www.hpc.cineca.it/systems/hardware/galileo100/, retrieved on February 21, 2025.

No. 2022WKWZA8 (“Immersed methods for multiscale and multiphysics problems (IMMEDIATE)”), and the support of the European Research Council (ERC) under the European Union’s Horizon 2020 research and innovation programme (call HORIZON-EUROHPC-JU-2023-COE-03, grant agreement No. 101172493 “dealii-X”). The authors are members of Gruppo Nazionale per il Calcolo Scientifico (GNCS) of Istituto Nazionale di Alta Matematica (INdAM).

Appendix A. Spectral equivalence of h-scaled mass matrices

We prove the spectral equivalence between the matrices $(h_\Gamma \mathsf{M}_\lambda)^{-1}$ and M_λ^{-2} when $d = 2$. In this case, the mass matrix M_λ is defined on the one-dimensional (closed) curve Γ_h. Recall that two families of SPD matrices $\{\mathsf{A}_l\}$ and $\{\mathsf{B}_l\}$ (parametrized by their dimension l) are said to be *spectrally equivalent* if there exist l-independent constants α and β with

$$0 < \alpha \leq \frac{\mathsf{w}^\mathsf{T}\mathsf{A}_l\mathsf{w}}{\mathsf{w}^\mathsf{T}\mathsf{B}_l\mathsf{w}} \leq \beta, \qquad \forall \mathsf{w} \neq 0.$$

We drop the subscript l. To show that

$$0 < \alpha \leq \frac{\mu^\mathsf{T}\mathsf{M}_\lambda^{-2}\mu}{\mu^\mathsf{T}(h_\Gamma\mathsf{M}_\lambda)^{-1}\mu} \leq \beta, \qquad \forall \mu \neq 0, \tag{A.1}$$

we first multiply and then divide the previous relation by $\mu^\mathsf{T}\mu$, so that it can be rewritten in terms of the Rayleigh quotients associated with the matrices $(h_\Gamma\mathsf{M}_\lambda)^{-1}$ and M_λ^{-2}. Since for a Hermitian matrix M, its Rayleigh quotient lies in the interval $[\lambda_{\min}(\mathsf{M}), \lambda_{\max}(\mathsf{M})]$, and the eigenvalues of the inverse of a matrix are the reciprocals of the eigenvalues of the original matrix, we get

$$\frac{\lambda_{\min}(h_\Gamma\mathsf{M}_\lambda)}{\lambda_{\max}(\mathsf{M}_\lambda^2)} \leq \frac{\mu^\mathsf{T}\mathsf{M}_\lambda^{-2}\mu}{\mu^\mathsf{T}(h_\Gamma\mathsf{M}_\lambda)^{-1}\mu} \leq \frac{\lambda_{\max}(h_\Gamma\mathsf{M}_\lambda)}{\lambda_{\min}(\mathsf{M}_\lambda{}^2)}. \tag{A.2}$$

Moreover, for a quasi-uniform subdivision in $\mathbb{R}^1$ of shape-regular elements[5], it holds

$$c h_\Gamma \leq \frac{\mu^\mathsf{T}\mathsf{M}_\lambda\mu}{\mu^\mathsf{T}\mu} \leq C h_\Gamma \qquad \forall \mu \in \mathbb{R}^l. \tag{A.3}$$

Noting that $\lambda(h_\Gamma\mathsf{M}_\lambda) = h_\Gamma\lambda(\mathsf{M}_\lambda)$ and $\lambda(\mathsf{M}_\lambda{}^2) = (\lambda(\mathsf{M}_\lambda))^2$, we use the above bounds for the eigenvalues in (A.2), which yields

$$0 < \frac{c}{C^2} \leq \frac{\mu^\mathsf{T}\mathsf{M}_\lambda^{-2}\mu}{\mu^\mathsf{T}(h_\Gamma\mathsf{M}_\lambda)^{-1}\mu} \leq \frac{C}{c^2}, \tag{A.4}$$

proving the spectral equivalence between the two matrices.

Appendix B. Inverse estimate

Lemma. *Let Λ_h be the space for the discrete Lagrange multiplier, defined in (25). Then, there exists a constant $C > 0$ independent of the mesh size h_Γ such that the following estimate holds:*

$$||\mu_h||_{-\frac{1}{2},\Gamma} \geq C h_\Gamma^{\frac{1}{2}} ||\mu_h||_{0,\Gamma} \qquad \forall \mu_h \in \Lambda_h. \tag{B.1}$$

Proof. In the case of H^1-conforming Lagrangian elements, by definition of dual norm, we have

$$||\mu_h||_{-\frac{1}{2},\Gamma} := \sup_{0 \neq z \in H^{\frac{1}{2}}(\Gamma)} \frac{\langle \mu_h, z\rangle_\Gamma}{||z||_{\frac{1}{2},\Gamma}} \geq \sup_{0 \neq z_h \in \Lambda_h} \frac{\langle \mu_h, z_h\rangle_\Gamma}{||z_h||_{\frac{1}{2},\Gamma}},$$

where the second inequality follows from the fact that $\Lambda_h \subset H^{\frac{1}{2}}(\Gamma)$. Therefore, upon choosing $z_h = \mu_h$, we obtain

$$||\mu_h||_{-\frac{1}{2},\Gamma} \geq \frac{||\mu_h||_{0,\Gamma}^2}{||\mu_h||_{\frac{1}{2},\Gamma}}.$$

Finally, using the following inequality

$$||\mu_h||_{\frac{1}{2},\Gamma} \leq c h_\Gamma^{-\frac{1}{2}} ||\mu_h||_{0,\Gamma},$$

which extends classical inverse inequalities (cfr. [60, Sect. 1.7]) from integer to real indices, gives the desired result. When Λ_h is the discontinuous space of piecewise constant functions, the result has been proven by Glowinski and Girault in [4] (Theorem 9). □

Appendix C. AMG parameters

The AMG parameter settings used in the numerical experiments are reported in Table C.1.

[5] Since $d = 2$, elements of Γ_h are one-dimensional intervals, for which the shape-regularity condition is automatically fulfilled.

Table C.1
Parameters for ML [54] (Trilinos 14.4.0).

Parameter	Value
Smoother	Chebyshev
Coarse solver	Amesos-KLU
Smoother sweeps	2
V-cycle applications	1
Aggregation threshold	10^{-4}
Max size coarse level	2000

References

[1] C.S. Peskin, The immersed boundary method, Acta Numerica. 11 (2002) 479–517. https://doi.org/10.1017/S0962492902000077
[2] J. Parvizian, A. Düster, E. Rank, Finite cell method, Comput. Mech. 41 (2007). https://doi.org/10.1007/s00466-007-0173-y
[3] E. Burman, S. Claus, P. Hansbo, M.G. Larson, A. Massing, CutFEM: discretizing geometry and partial differential equations, Int. J. Numer. Methods Eng. 104 (7) (2015) 472–501. https://doi.org//10.1002/nme.4823
[4] V. Girault, R. Glowinski, Error analysis of a fictitious domain method applied to a Dirichlet problem, Japan J. Ind. Appl. Math. 12 (3) (1995) 487–514. https://doi.org/10.1007/BF03167240
[5] D. Boffi, L. Gastaldi, A fictitious domain approach with Lagrange multiplier for fluid-structure interactions, Numer. Math. 135 (3) (2017) 711–732. https://doi.org/10.1007/s00211-016-0814-1
[6] G. Hou, J. Wang, A. Layton, Numerical methods for fluid-structure interaction - a review, Commun. Comput. Phys. 12 (2) (2012) 337–377. https://doi.org/10.4208/cicp.291210.290411s
[7] L. Heltai, N. Rotundo, Error estimates in weighted Sobolev norms for finite element immersed interface methods, Comput. Math. Appl. 78 (11) (2019) 3586–3604. https://doi.org//10.1016/j.camwa.2019.05.029
[8] D. Boffi, A. Cangiani, M. Feder, L. Gastaldi, L. Heltai, A comparison of non-matching techniques for the finite element approximation of interface problems, Comput. Math. Appl. 151 (2023) 101–115.
[9] D. Boffi, F. Credali, L. Gastaldi, Quadrature error estimates on non-matching grids in a fictitious domain framework for fluid-structure interaction problems, arXiv:2406.03981 (2024).
[10] D. Boffi, F. Credali, L. Gastaldi, On the stability and conditioning of a fictitious domain formulation for fluid-structure interaction problems, arXiv:2505.05228 (2025).
[11] E. Burman, P. Hansbo, Fictitious domain finite element methods using cut elements: I. A stabilized Lagrange multiplier method, Comput. Methods Appl. Mech. Eng. 199 (2010) 2680–2686.
[12] D. Boffi, F. Credali, L. Gastaldi, On the interface matrix for fluid-structure interaction problems with fictitious domain approach, Comput. Methods Appl. Mech. Eng. 401 (2022) 115650. https://www.sciencedirect.com/science/article/pii/S0045782522006053. https://doi.org//10.1016/j.cma.2022.115650
[13] R. Krause, P. Zulian, A parallel approach to the variational transfer of discrete fields between arbitrarily distributed unstructured finite element meshes, SIAM J. Sci. Comput. 38 (3) (2016) C307–C333. https://doi.org/10.1137/15M1008361
[14] M. Feder, L. Heltai, M. Kronbichler, P. Munch, Matrix-free implementation of the non-nested multigrid method, arXiv:2412.10910 (2024).
[15] M. Benzi, G.H. Golub, J. Liesen, Numerical solution of saddle point problems, Acta Numerica 14 (2005) 1–137. https://doi.org/10.1017/S0962492904000212
[16] J. Maryska, M. Rozložník, M. Tuma, Schur complement systems in the mixed-hybrid finite element approximation of the potential fluid flow problem, SIAM J. Sci. Comput. 22 (2000) 704–723. https://doi.org/10.1137/S1064827598339608
[17] D. Boffi, F. Brezzi, M. Fortin, Mixed Finite Element Methods and Applications, Springer Series in Computational Mathematics, Springer Berlin Heidelberg, 2013. https://books.google.it/books?id=mRhAAAAAQBAJ.
[18] H.C. Elman, D.J. Silvester, A.J. Wathen, Finite Elements and Fast Iterative Solvers: with Applications in Incompressible Fluid Dynamics, Oxford series in Numerical mathematics and scientific computation, Oxford University Press, 2nd Edition, 2014. https://books.google.it/books?id=9zSTAwAAQBAJ.
[19] F. de Prenter, C.V. Verhoosel, E.H. van Brummelen, Preconditioning immersed isogeometric finite element methods with application to flow problems, Comput. Methods Appl. Mech. Eng. 348 (2019) 604–631. https://www.sciencedirect.com/science/article/pii/S0045782519300556. https://doi.org//10.1016/j.cma.2019.01.030
[20] S. Gross, A. Reusken, Analysis of optimal preconditioners for CutFEM, Numer. Linear Algebra Appl. 30 (5) (2023) e2486. https://onlinelibrary.wiley.com/doi/abs/10.1002/nla.2486. https://doi.org//10.1002/nla.2486
[21] F. de Prenter, C.V. Verhoosel, G.J. van Zwieten, E.H. van Brummelen, Condition number analysis and preconditioning of the finite cell method, Comput. Methods Appl. Mech. Eng. 316 (2017) 297–327.
[22] M. Kuchta, M. Nordaas, J.C.G. Verschaeve, M. Mortensen, K.-A. Mardal, Preconditioners for saddle point systems with trace constraints coupling 2D and 1D domains, SIAM J. Sci. Comput. 38 (6) (2016) B962–B987.
[23] A. Budiša, X. Hu, M. Kuchta, K.-A. Mardal, L. Zikatanov, Rational approximation preconditioners for multiphysics problems, in: International Conference on Numerical Methods and Applications, Springer, 2022, pp. 100–113.
[24] Y. Li, L.T. Zikatanov, C. Zuo, Reduced Krylov basis methods for parametric partial differential equations, arXiv:2405.07139 (2024).
[25] A.B. Fatemeh Panjeh, M. Benzi, Iterative methods for double saddle point systems, SIAM J. Matrix Anal. Appl. 39 (2) (2018) 902–921. https://doi.org/10.1137/17M1121226
[26] F.P.A. Beik, M. Benzi, An augmented Lagrangian-based preconditioning technique for a class of block three-by-three linear systems, Appl. Math. Lett. 149 (2024) 108903. https://www.sciencedirect.com/science/article/pii/S089396592300335X. https://doi.org//10.1016/j.aml.2023.108903
[27] F.P.A. Beik, M. Benzi, Preconditioning techniques for the coupled Stokes-Darcy problem: spectral and field-of-values analysis, Numer. Math. 150 (2) (2022) 257–298. https://doi.org/10.1007/s00211-021-01267-8
[28] F. Bakrani, L. Bergamaschi, A. Martinez, M. Hajarian, Some preconditioning techniques for a class of double saddle point problems, Numer. Linear Algebra Appl. 31(4), e2551 (2024). https://doi.org/10.1002/nla.2551
[29] A. Ramage, E.C. Gartland, A preconditioned nullspace method for liquid crystal director modeling, SIAM J. Sci. Comput. 35 (1) (2013) B226–B247. https://doi.org/10.1137/120870219
[30] M. Benzi, F.P.A. Beik, Uzawa-type and augmented Lagrangian methods for double saddle point systems, *In: D. Bini, F. Di Benedetto, E. Tyrtyshnikov, and M. Van Barel (Eds.),* Structured Matrices in Numerical Linear Algebra: Analysis, Algorithms and Applications, *Springer INdAM Series* 30 (2019) 215–236.
[31] A.B. Fatemeh Panjeh, M. Benzi, Block preconditioners for saddle point systems arising from liquid crystal directors modeling, Calcolo 55:29 (2018). https://api.semanticscholar.org/CorpusID:2541346886.
[32] J.-L. Zhu, Y.-J. Wu, A.-L. Yang, A two-parameter block triangular preconditioner for double saddle point problem arising from liquid crystal directors modeling, Numer. Algorithms 89 (2022) 987–1006. https://doi.org/10.1007/s11075-021-01142-5
[33] F. Chen, B.-C. Ren, A modified alternating positive semidefinite splitting preconditioner for block three-by-three saddle point problems, ETNA - Electron. Trans. Numer. Anal. 58 (2022) 84–100. https://doi.org/10.1553/etna_vol58s84
[34] D. Boffi, F. Credali, L. Gastaldi, S. Scacchi, A parallel solver for FSI problems with fictitious domain approach, Math. Comput. Appl. 28 (2) (2023) 59.

[35] D. Boffi, F. Credali, L. Gastaldi, S. Scacchi, A parallel solver for fluid-structure interaction problems with Lagrange multiplier, Math. Comput. Simul. 220 (2024) 406–424. https://www.sciencedirect.com/science/article/pii/S0378475424000399. https://doi.org//10.1016/j.matcom.2024.01.027
[36] N. Alshehri, D. Boffi, C. Chaoveeraprasit, Multigrid preconditioning for FD-DLM method in elliptic interface problems, arXiv:2503.00146 (2025).
[37] C. Wang, P. Sun, An augmented Lagrangian Uzawa iterative method for solving double saddle-point systems with semidefinite (2,2) block and its application to DLM/FD method for elliptic interface problems, Commun. Comput. Phys. 30 (1) (2021) 124–143. https://doi.org//10.4208/cicp.OA-2020-0084
[38] S. Berrone, A. Bonito, R. Stevenson, M. Verani, An optimal adaptive fictitious domain method, Math. Comput. 88 (2017) 2101–2134. https://api.semanticscholar.org/CorpusID:52023195.
[39] M. Benzi, M.A. Olshanskii, An augmented Lagrangian-based approach to the Oseen problem, SIAM J. Sci. Comput. 28 (6) (2006) 2095–2113. https://doi.org/10.1137/050646421
[40] M. Benzi, M.A. Olshanskii, Z. Wang, Modified augmented Lagrangian preconditioners for the incompressible Navier-Stokes equations, Int. J. Numer. Methods Fluids 66 (4) (2011) 486–508. https://doi.org//10.1002/fld.2267
[41] Y. Saad, A flexible inner-outer preconditioned GMRES algorithm, SIAM J. Sci. Comput. 14 (2) (1993) 461–469. https://doi.org/10.1137/0914028
[42] D. Arndt, W. Bangerth, D. Davydov, T. Heister, L. Heltai, M. Kronbichler, M. Maier, J.-P. Pelteret, B. Turcksin, D. Wells, The deal.II finite element library: design, features, and insights, Comput. Math. Appl. 81 (2021) 407–422.
[43] D. Arndt, W. Bangerth, M. Bergbauer, M. Feder, M. Fehling, J. Heinz, T. Heister, L. Heltai, M. Kronbichler, M. Maier, P. Munch, J.-P. Pelteret, B. Turcksin, D. Wells, S. Zampini, , J. Numer. Math. 31 (3) (2023) 231–246. https://dealii.org/deal95-preprint.pdf. https://doi.org/10.1515/jnma-2023-0089
[44] F. Brezzi, On the existence, uniqueness and approximation of saddle-point problems arising from lagrangian multipliers, R.A.I.R.O. Anal. Numérique 8 (1974) 129–151. https://api.semanticscholar.org/CorpusID:41648116.
[45] T.A. Davis, Algorithm 832: UMFPACK V4.3—an unsymmetric-pattern multifrontal method, ACM Trans. Math. Softw. 30 (2) (2004) 196–199. https://doi.org/10.1145/992200.992206
[46] J.S. Howell, N.J. Walkington, Inf-sup conditions for twofold saddle point problems, Numer. Math. 118 (4) (2011) 663–693. https://doi.org/10.1007/s00211-011-0372-5
[47] D. Boffi, L. Gastaldi, On the quadrilateral Q2/P1 element for the Stokes problem, Int. J. Numer. Methods Fluids 39 (11) (2002) 1001–1011. https://doi.org//10.1002/fld.358
[48] T. Heister, G. Rapin, Efficient augmented Lagrangian-type preconditioning for the Oseen problem using Grad-div stabilization, Int. J. Numer. Methods Fluids 71 (1) (2013) 118–134. https://doi.org//10.1002/fld.3654
[49] M.A. Olshanskii, A. Reusken, Grad-div stabilization for Stokes equations, Math. Comput. 73 (2004) 1699–1718.
[50] A. Greenbaum, V. Pták, Z. Strakoš, Any nonincreasing convergence curve is possible for GMRES, SIAM J. Matrix Anal. Appl. 17 (3) (1996) 465–469. https://doi.org/10.1137/S0895479894275030
[51] B. Faermann, Localization of the Aronszajn-Slobodeckij norm and application to adaptive boundary elements methods. part I. The two-dimensional case, IMA J. Numer. Anal. 20 (2) (2000) 203–234. https://doi.org/10.1093/imanum/20.2.203
[52] S. Bertoluzza, Localization of trace norms in two and three dimensions, arXiv preprint arXiv:2312.01101 (2023).
[53] D.S. Malkus, Eigenproblems associated with the discrete LBB condition for incompressible finite elements, Int. J. Eng. Sci. 19 (10) (1981) 1299–1310. https://doi.org//10.1016/0020-7225(81)90013-6
[54] M.A. Heroux, R.A. Bartlett, V.E. Howle, R.J. Hoekstra, J.J. Hu, T.G. Kolda, R.B. Lehoucq, K.R. Long, R.P. Pawlowski, E.T. Phipps, A.G. Salinger, H.K. Thornquist, R.S. Tuminaro, J.M. Willenbring, A. Williams, K.S. Stanley, An overview of the trilinos project, ACM Trans. Math. Softw. 31 (3) (2005) 397–423. https://doi.org/10.1145/1089014.1089021
[55] S. Balay, S. Abhyankar, M.F. Adams, J. Brown, P. Brune, K. Buschelman, L. Dalcin, V. Eijkhout, W.D. Gropp, D. Kaushik, M.G. Knepley, L.C. McInnes, K. Rupp, B.F. Smith, S. Zampini, H. Zhang, PETSc web page, 2015, (http://www.mcs.anl.gov/petsc).
[56] W. Gropp, E. Lusk, N. Doss, A. Skjellum, A high-performance, portable implementation of the MPI message passing interface standard, Parallel Comput. 22 (6) (1996) 789–828. https://doi.org//10.1016/0167-8191(96)00024-5
[57] H.C. Elman, Preconditioning for the steady-State Navier–Stokes equations with low viscosity, SIAM J. Sci. Comput. 20 (4) (1999) 1299–1316. https://doi.org/10.1137/S1064827596312547
[58] C.C. Paige, M.A. Saunders, Solution of sparse indefinite systems of linear equations, SIAM J. Numer. Anal. 12 (4) (1975) 617–629. https://doi.org/10.1137/0712047
[59] P.E. Farrell, L. Mitchell, F. Wechsung, An augmented Lagrangian preconditioner for the 3D stationary incompressible Navier–Stokes equations at high Reynolds number, SIAM J. Sci. Comput. 41 (5) (2019) A3073–A3096. https://doi.org/10.1137/18M1219370
[60] A. Ern, J.L. Guermond, Theory and Practice of Finite Elements, Appl. Math. Sci. 159, Springer-Verlag, New York, 2004.